PET/MR: Basics and New Developments

9

Magdy M. Khalil

Contents

Abstract

It has become evident that hybrid modalities are one of the most important technical and clinical achievements in clinical imaging over the last two decades. This has impacted significantly many aspects of patient diagnosis, stratification, prognosis, and treatment strategies. After the advent of SPECT/CT and PET/CT to the clinical arena, PET/MR was introduced shortly afterward with real simultaneous capabilities and additional features mainly characterized by the inherent differences between MR and CT imaging techniques. In this chapter, objectives were made to describe the technical challenges behind the hybridization of PET and MR in one imaging system especially if the aim is to produce a simultaneous data acquisition. Different commercially available PET/MR systems were also described along with their specific characteristics, geometry, and design. The use of new PET detector technology was one of the reasons beyond the success of hybrid PET/MR. Thus, some details were provided for different types of crystals and light photosensors along with other interfering variables with MR detector components. Attenuation and motion correction in PET/MR imaging were reviewed with recent tips on approaches devised and their relative merits. Small animal PET/MR was outlined as well. Challenges, opportunities, and future directions were highlighted at the end of the chapter.

M.M. Khalil, PhD
Medical Biophysics, Department of Physics,
Faculty of Science, Helwan University, Cairo, Egypt
e-mail: magdy_khalil@hotmail.com

M.M. Khalil (ed.), *Basic Science of PET Imaging*, DOI 10.1007/978-3-319-40070-9_9

9.1 Introduction

In the last two decades, there was a large interest in multimodality hybrid imaging. The combination of functional imaging with anatomical imaging modalities was so attractive to the nuclear medicine community on both clinical and technical levels. The functional imaging is provided by nuclear medicine imaging techniques that include single-photon emission computed tomography (SPECT) and positron emission tomography (PET), while the latter is the main focus of morphological diagnostic imaging such as x-ray computed tomography (CT) and magnetic resonance imaging (MRI). The advent of hybrid multimodal SPECT/CT, PET/CT, and PET/MR and introduction into the clinic were so close in time such that we can call the last two decades the age of hybrid imaging.

The rationale behind that interest was to gain the strength of each imaging modality, to reveal the maximum information about human diseases in one imaging session, to shorten the diagnostic workup, and to accelerate the treatment decision-making process. This obviously has several features and advantages in patient management and clinical outcome. The morphological modalities have several quality parameters such as high spatial and contrast resolution providing high anatomical details of patient morphology. Nuclear medicine and molecular imaging techniques, on the other hand, have much better molecular sensitivity but poor spatial resolution in comparison to the structural modalities. The tracer or radiopharmaceutical can be injected in nano- or picomolar molar concentration without disturbing the physiological system or molecular/cellular pathways [1–3]. PET tracers lie in a wide range library, and tailoring new probes able to decipher a biological question or investigate a particular molecular pathway can be designed. The advent of PET/CT and SPECT/CT to the clinical arena and their wide spread in routine practice have encouraged researchers to copy the same experience in introducing PET/MR imaging systems into the clinic.

First attempts to combine PET with MR were focused on preclinical system model in the 1990s, whereas it was not until 2006 that the first integral simultaneous PET/MR (BrainPET, Siemens Healthcare, Inc.) imaging of the brain took place [4]. Combining PET with MRI in the same scanner has several diagnostic benefits and clinical advantages. A great soft tissue contrast can be achieved with MRI sequences avoiding the use of ionizing radiation imparted by CT imaging procedures. MRI has also a functional part but with sensitivity significantly lower than PET; it is in the range of 10^{-5} mol/L, while for molecular PET imaging lies in the range of 10^{-9}–10^{-12} mol/L. MRI can provide functional information such as tissue perfusion, diffusion, and spectroscopy in addition to other benefits such as motion correction and anatomy-based image reconstruction as well as reduction of positron range effects and improvement in spatial resolution [5].

There are many technical and operational differences between PET/CT and PET/MR, and this obviously comes from the different underlying principles of CT and MR imaging components. These are but not limited to image acquisition, data reconstruction and processing, clinical examinations and data flow, contrast agents and contraindications, scan speed and patient throughput, radiation exposure to patients and staff and some other variables that include reimbursement and examination fees, etc. [6]. PET/MR examinations have successfully been introduced into the clinic, and extensive research work is being carried out to assess its effectiveness in routine practice of medical diagnosis. Nevertheless, the clinical utility of simultaneous PET/MR may be seen more effective in organ-specific, disease-specific, and pediatric-related applications or in those patients where their follow-up would be of important clinical value [7]. Eventually, the marathon of PET/CT and PET/MR has started trying to address some questions such as whether PET/MRI will be able to provide incremental diagnostic accuracy, an incremental impact on management, or an incremental impact on patient outcome compared with PET/CT [8].

9.2 PET/CT

One of the ideal design goals of a hybrid imaging modality is to acquire diagnostic information at the same time without compromising patient

comfort or prolonging acquisition times with little or no mutual interference of one system to another. Up to the moment of writing this chapter, there is no commercial hybrid system able to acquire PET signal as well as CT or MRI information at the same time using the same detector module. However, the commercial designs available so far are built on the notion of simultaneously acquiring the different diagnostic signals using two different detector systems or sequentially acquiring one after the other. The first PET/CT design has incorporated a single-slice spiral CT scanner (Somatom AR.SP; Siemens Medical Solutions, Forchheim, Germany) and a rotating ECAT ART scanner (CTI PET Systems, Knoxville, TN) [9]. The PET scanner consisted of two opposing detector banks leaving a physical gap between the two detectors. This gap was suggested to be a useful space for incorporating a CT scanner so that anatomical information can be obtained. While this idea was not practically applicable due to the heavy elements of CT imaging system, it was inspiring to design a hybrid PET/CT such that both can be located side by side [10].

The first PET/CT prototype was funded by the National Institutes of Health (NIH) and designed such that the CT and PET components rotated as a single assembly acquiring CT and PET data sequentially. The entire rotating assembly was housed within a single gantry cover. This prototype became operational in 1998 and subsequently clinically evaluated at the University of Pittsburgh [9].

An increased radiation dose especially for repeated measurements of therapy monitoring is one of the PET/CT drawbacks that might have a potential risk implication. This is particularly critical in pediatric patients and response monitoring. Poor soft tissue contrast is also a limitation in some clinical examinations such as brain, prostate, abdomen, and breast imaging that may require an injection of contrast agents. Similarly, PET/CT in small animal research has some limitations as increased dose to the animal may contribute to the total radiation burden, creating a confounding or interfering effect to the drug under investigation. The poor soft tissue contrast provided by CT especially in the era of developing new specific radiotracers that need clear anatomical details is also a clear drawback in animal research. Physics and instrumentation of PET and PET/CT are described in Chap. 8.

9.3 PET/MR: System Design

Attempts to manufacture PET/MR imaging systems were based on two distinct designs, sequential versus concurrent (or simultaneous) data acquisition. The main difference in both systems is the way how the two detector systems are located in relation to each other. Sequential design is straightforward, is less integrated, is not temporally correlated, and requires less hardware modifications, and two major vendors have adopted that design.

One design was implemented by Philips Healthcare (The Ingenuity TF PET/MR, Cleveland, OH) and fabricated such that the PET and MR scanners are located in the same imaging room and able to perform a time of flight (TOF) data acquisition [11]; see Fig. 9.1. The PET and MR scanners are axially aligned at opposite ends of a linearly translating bed and the centers of the scanners are 4.2 m apart. The room dimension requirement is relatively large measuring 4.5 × 13 m. The chance of patient motion between the two scans still exists, and the acquisition time is also compromised and varies according to the clinical question. The PET detector ring is surrounded by additional shielding (i.e., laminated steel shield), and each photomultiplier is inserted in a mu-metal case [12].

The other sequential system was adopted by GE Healthcare (Milwaukee, USA) where two scanners, one hybrid (PET/CT) and one standalone (MR), are separated and installed in two different rooms as shown in Fig. 9.2. The two separate systems have the same imaging table that can be transferred from one room to another achieving a multimodality sequential PET/CT and MR diagnostic examination [13]. This system has minimal if no mutual interference between the two scanning units, and therefore image quality and quantitative accuracy are maintained. While this approach provides more flexibility to use the two imaging systems separately and independently and can be optimized to select those patients who

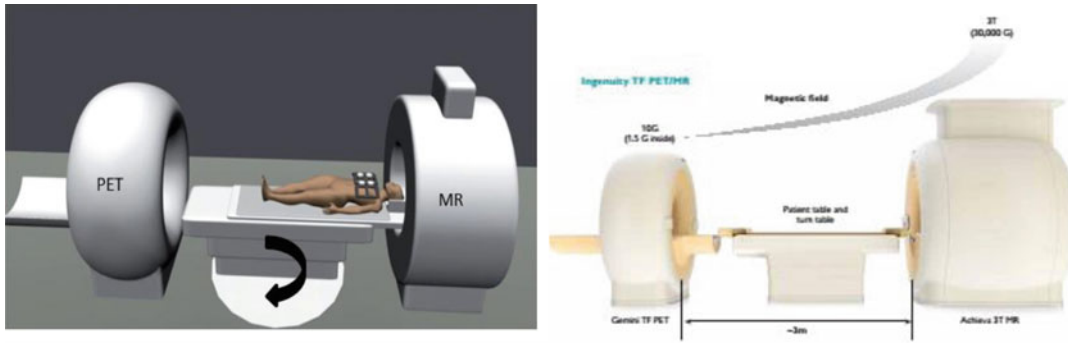

Fig. 9.1 The model implemented in Philips PET/MR system. The two modules are located at adequate far distant apart, minimizing mutual interference between the two systems, and data are acquired in a sequential mode (Image is courtesy of Philip Health Care, Inc.)

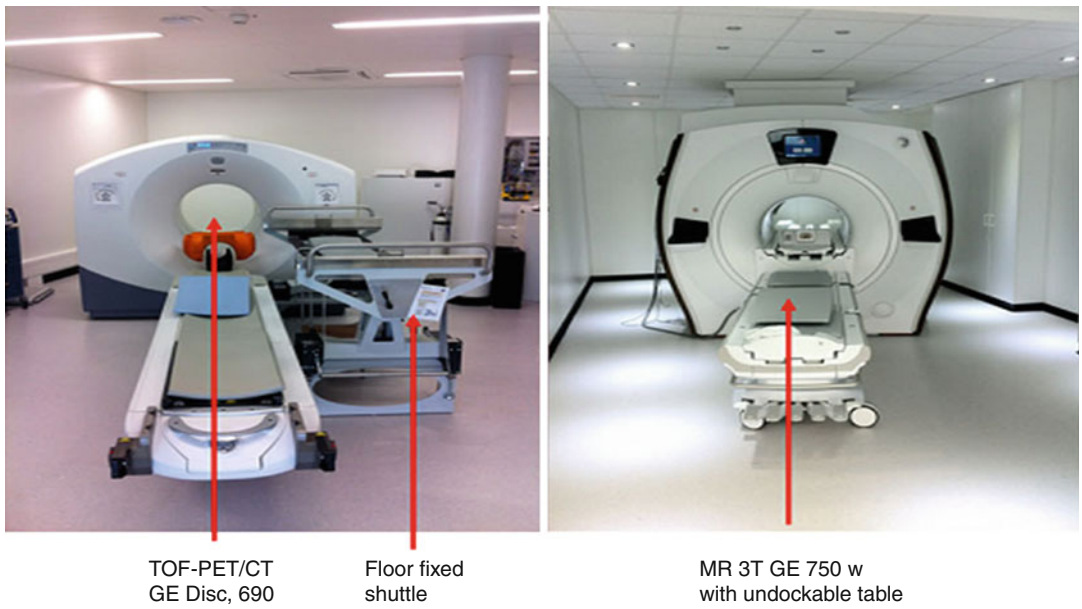

Fig. 9.2 First PET/CT/MR version adopted by GE Healthcare using 3 T MRI system and a TOF-PET/CT in two rooms directly adjacent to each other (Taken from Ref. [14] with permission)

need PET/CT or a combination of PET/CT/MR, it remains an additional source of radiation due to CT part of the examination besides likelihood of patient motion that causes undesired imaging artifacts [13].

On the other hand, the concurrent PET/MR systems provide a simultaneous data acquisition preserving the temporal and spatial correlation between the two data sets. This approach is either a PET insert located inside the magnet bore or alternatively a PET detector fully integrated into an MR scanner [14–16]. Initial attempts were focused on the insert type to reduce positron range and thus improved spatial resolution of the PET data. However, some challenges are needed to be tackled due to the presence of PET scintillator and associated electronics within the MR field of view. Magnetic susceptibility of the PET components needs to be minimized; otherwise, a deleterious influence on the static field would impact data acquisition and image quality. Therefore, shielding of the magnetic-sensitive components

would be essential to maintain field homogeneity and minimize cross talk interference. Alternatively, using magnetic insensitive PET components or placing the PET electronics outside the fringe field would be an alternative option. Size constraints would impact negatively on PET detection sensitivity as the axial extent would be limited as well.

The insert-type PET/MR provides a reduced total acquisition time, minimizes likelihood of patient motion, and doesn't require major modifications in the MR magnet configurations. The PET insert design is successful in scanning small objects like small animals' imaging, brain, and extremities but of limited feasibility in whole-body PET/MR due to space limitations that created in the magnet bore. In addition, removing the insert would make the MR to work as a single imaging module providing a cost-effective less integrated option [6, 17].

In comparison to PET/CT, the integrated design is a unique feature that characterizes PET/MR over PET/CT in providing a perfect intrinsic co-registration. Reduction of the total acquisition time is also another advantage provided by simultaneous PET/MR systems in comparison to sequential design. However, integrated design is more challenging and expensive and requires major changes and modification when compared to separate scanning units. The first hybrid whole-body PET/MR scanner (Biograph mMR, Siemens Healthcare) was installed in 2010. It is based on the Siemens Verio 3-T MRI scanner using avalanche photodiode with water cooling mechanism. The bore has been reduced due to this integration from 70 to 60 cm and the PET detector was placed behind the RF coil [14] (Fig. 9.3).

Note that larger-bore magnet is also challenging because the gradient system pays a steep price and performance penalty for its increased size as power requirements go steeply with radius and manufacturing tolerances for gradient shielding become much more demanding [18]. Having the PET detector behind the RF coils allows for reduction of interference with excitation pulses, but temperature and other gamma rays' attenuation and photon scatter need to be addressed. A split magnet is an approach that also permits PET detector integration and facilitates coupling of the processing electronics, rendering the signal more robust to interference [19].

The other simultaneous PET/MR system recently reported by GE Healthcare is the Signa TOF-PET/MR. The MR component is based on the GE 3-T Discovery 750w MRI system which has an inner bore of 70 cm diameter. The PET scanner has a transverse FOV of 60 cm and an axial extent of 25 cm (89 slices) and comprises of five rings of 112 detector blocks. Each block consists of 4 × 9 array of lutetium based with similar density to LYSO crystal [3.95 mm (transverse) × 5.3 mm (axial) × 25 mm^3 (depth)] coupled to 1 × 3 arrays of SiPM devices [20]. The PET detectors' modules are centered inside the MR gradient set and mounted on the outside of the RF body coil that provides additional space to accommodate the PET detector ring with a 60-cm patient bore. The PET detector relies on SiPM photodetector technology and uses a custom-made ASIC for readout, which permits gain adjustment on the individual pixel level.

Preliminary system performance showed 4-mm spatial resolution (using line source), 10.5 % energy resolution, 22.5 kcps MBq^{-1} system sensitivity based on NEMA measurements, and 215 kcps at 17 kBq/ml activity concentration [21]. Initial evaluation resulted in roughly more than 50 % of dose reduction can be clinically achieved [22]. The relatively high sensitivity is owing to large axial extent (25 cm), detector depth, and recovery of events occurred by Compton interactions within the detector [23]. The system is shown in Fig. 9.4. The three major vendors of PET/MR systems are summarized in Table 9.1.

9.3.1 PET/MR Technical Challenges

Allocation of the PET detector within the magnetic bore and removing mutual interference with MRI components are the two initial but major issues that need to be tackled before realizing an integrated hybrid PET/MR system. The magnetic field has its well-known degrading effect on the photomultiplier tube (PMT). The vacuum of the PMT

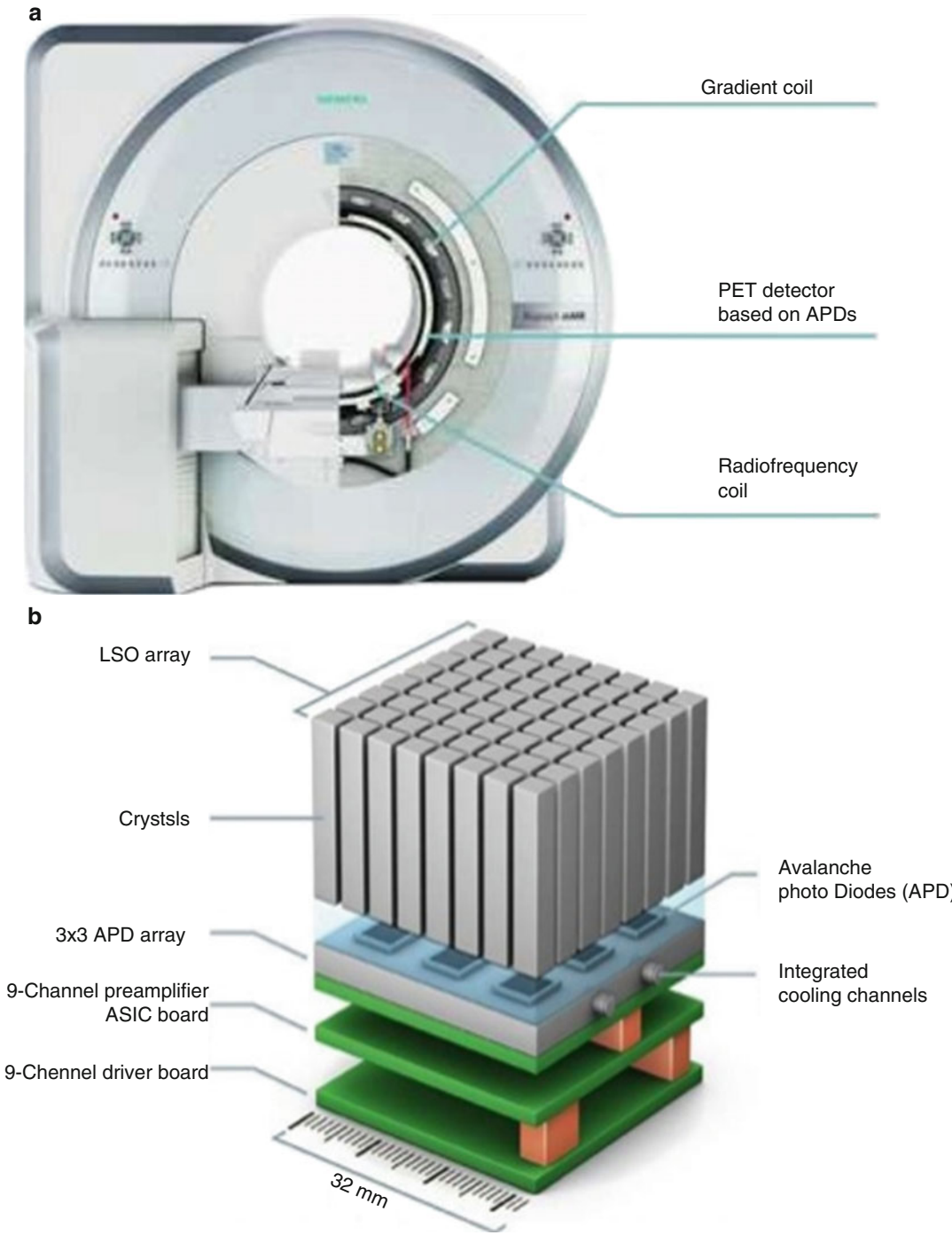

Fig. 9.3 (**a**) Cross section of the Siemens fully integrated PET/MR (Biograph mMR, Siemens Healthcare, Inc.). (**b**) PET detector module showing the segmented LSO crystal coupled to APD with the integrated cooling system (Images are courtesy of Siemens Healthcare)

Fig. 9.4 GE Healthcare TOF-PET/MR integrated system (i.e., Signa) that simultaneously acquires PET and MR signals. It combines simultaneous data acquisition from GE's latest 3.0 T MR750w and SiPM-based PET technology

Table 9.1 Summary of the PET/MR systems released by the three major manufacturers

PET/MR system	Biograph mMR (Siemens)	Ingenuity TF (Philips)	Discovery PET/CT 690 + MR 750 (GE)
PET system			
Crystal material	LSO	LYSO	LYSO
Crystal elements dimension	$4 \times 4 \times 20$ mm^3	$4 \times 4 \times 22$ mm^3	$4.7 \times 6.3 \times 25$ mm^3
Photomultipliers	No, 4032 APDs	420	1024
Ring diameter	65.6 cm	90.3 cm	88.6 cm
Transaxial FoV	59.4 cm	67.6 cm	70 cm
Axial FoV	25.8 cm	18.0 cm	15.7 cm
Energy window	430–610 keV	460–665 keV	425–650 keV
Coincidence window	5.9 ns	6 ns	4.9 ns
Time of flight	No	Yes	Yes
MR system			
Field strength	3 Tesla	3 Tesla	3 Tesla
Bore diameter	60 cm	60 cm	60 cm
Max FoV	$50 \times 50 \times 45$ cm^3	$50 \times 50 \times 45$ cm^3	$48 \times 48 \times 48$ cm^3
Field homogeneity (40 cm^3)	0.25 ppm	0.5 ppm	0.25 ppm
PET/MR			
Acquisition	Simultaneous	Sequential (same room)	Sequential (2 separate rooms)
PET attenuation correction	MR-based	MR-based	CT-based

Namely, Biograph mMR from Siemens, Ingenuity TF from Philips, and the trimodality hybrid system from GE Healthcare that consists of Discovery PET/CT and MR 750 [24]. The GE Healthcare Signa PET/MR system is described in the text

has several accelerating dynodes of varying potential difference. The photoelectrons emitted from the tube cathode are amplified through this process which is very sensitive to magnetic fields. The existence of PMT-based PET detector in the MRI magnetic fields results in a potential signal deterioration and distorted PET image. Another undesired feature of the PMT is the bulky structure that doesn't facilitate an easy integration inside the magnet core.

The strong static magnetic field and abrupt changes in the gradient magnetic field in addition to the radio-frequency pulse are major MRI elements that influence the PET detector system. Furthermore, the radio frequency and its rapidly changing pulses create eddy currents in any conductive material present in the field in addition to mechanical and vibrational noise [25–27]. Eddy current is a phenomenon created when a time-varying magnetic flux through a closed circuit produces an electromotive force proportional to its rate of change in a close proximity conductive material. It results from the excitation RF pulse and the rapidly changing gradient coil and could have several imaging drawbacks like a spatially variant phase change of the resonance signal, or the associated field will alter the spatial encoding of the signal leading to a distortion of the reconstructed images [24].

The presence of PET electronics in the magnetic field of the MR system has also its own drawbacks. It is important to maintain the magnetic field homogeneity avoiding any source that affects this uniform pattern. PET electronics including crystal, front-end electronics, any RF or radiation shielding, and particularly ferromagnetic components could potentially affect field homogeneity and linearity of the coil gradient system. Therefore, the shielding material should be carefully selected and optimized for data acquisition and elimination of imaging artifacts and data distortion [28].

In terms of image quantitation, attenuation correction is one of the major challenges that need to be properly tackled in order to achieve reliable (absolute or relative) quantitative measures. Other aspects that are tightly associated with MR imaging are the presence of metallic components and bony structures that have no significant information on the MR images. MR hardware is also critical in photon attenuation and could compromise correction techniques. These points will be discussed later.

9.3.2 What Is the Solution Then?

To solve the aforementioned problems, there were two major but different approaches that were taken into consideration. One of them was to keep the PMT at adequate distance away from the MR interfering signal. The distance was calculated such that the fringe magnetic field drops below 10 mT and the scintillation light was transmitted through lines of optical fibers. The first simultaneous preclinical prototype was built analogous to that way and consisted of a ring of forty eight $2\times2\times10$ mm^3 lutetium oxyorthosilicate (LSO) crystals of 38-mm inner diameter, implementing a one-to-one pixel coupling to three multichannel PMTs (MC-PMT) connected via (2 mm diameter and 4 m long) double clad optical fibers [29].

Shielding the PMT using steel or mu-metal is effective in weak magnetic field but fails in the strong fields used in MRI imaging systems. Using long optical fibers was not a perfect solution and showed some drawbacks such as loss of light signal (five to tenfold), deterioration of energy resolution, as well as degradation of timing resolution [30]. However, recent work on this area has also been extended to use a 90° light guide to transfer the light from the crystal to the optical fibers permitting the PMT to be placed in a magnetic-shielded region of 0.3 mT behind the yoke [31]. A reduction of light loss was achieved by newly developed flexible optical fiber bundle-based block detectors, employing them in a high-resolution integrated PET/MRI system [31].

The other solution was to use solid-state semiconductor photodetector such as avalanche photodiode (APD) or silicon photomultiplier (SiPM) that are insensitive to high magnetic field of the MR scanner [32, 33]. Avalanche photodiodes can operate in MR magnetic field without apparent distortion and have been successfully coupled to bismuth germinate (BGO) or cerium-doped lutetium oxyorthosilicate (LSO) crystals. The size of the APD is very small, and thus a compact PET/MR design can be manufactured using this type of solid-state photodetectors. The timing resolution in the range of nanoseconds and thus TOF is not possible. However, SiPM has been emerging as a potential and better candidate due to its signal-to-noise (SNR) ratio, higher gain, and timing resolution in the range of sub-nanosecond, and thus time of flight can be realized [34]. Further details on those types of photodetectors are discussed in Sect. 9.2.5.

9.3.3 PET Detector in PET/MR

The current generation of PET imaging systems relies on the full ring design that provides a simultaneous data acquisition of all projection angles at the same time. So detector rotation is eliminated and count sensitivity is greatly improved in comparison to older versions such as partial ring or single ring design. As discussed in Chap. 8, the block detector is the conventional and most adopted standard detector design used in PET imaging scanners. The scintillator block is viewed from the backside normally by 4 PMT that read out the light signal converting it into electric current for further processing and event spatial, temporal, and energy determination.

TOF-PET scanners do utilize the new advances in scintillation crystals, electronics, and computer technology by exploiting the full potential of PET in improving SNR [35]. TOF was not the only feature, but in the last decade, there were several developments in PET imaging such as an improved detector technology, electronic circuitry, data acquisition boards, processing and computer workstations, image reconstruction, and modeling of image-degrading factors, and all of these resulted in overall improved system performance and diagnostic accuracy.

9.3.4 Crystal

Scintillation crystal is the first component that receives the coincidence photons during the scanning process. The crystal role is to shift the wavelength of the incident energy into higher values that permit further downstream signal processing. This is because the light quanta emitted from the crystal have lower energy (higher wavelength) than the incident radiation beam. BGO crystal was the conventional detector material used for many years in PET systems due to its efficient stopping power and nonhygroscopic properties in comparison to Na(Tl) crystal. The scintillation crystal in PET/MR system should be carefully selected so that any magnetic susceptibility must be avoided (i.e., the degree of magnetization of a material in response to an applied magnetic field) [36]. BGO, LSO, and LYSO crystals were found to have lower magnetic susceptibility, but GSO and LGSO are not appropriate and can cause MRI artifacts. The former group is the most common in the current PET/CT and PET/MR systems. Currently, the most preferred crystal type is the LSO-type crystals due to high light output, good detection efficiency, and short decay constant that permits TOF applications.

9.3.5 Photodetectors

9.3.5.1 Photomultiplier Tube (PMT)

The most commonly used photosensors in gamma camera and PET imaging systems are the PMTs due to its high gain that lie in the range of 10^5–10^7 in addition to the fast timing characteristics. It is manufactured in wide range of geometries, sizes, and designed base on vacuum tube technology that improved significantly over the years. Some of these improvements are better timing performance, enhanced quantum efficiency, and developments of multichannel and position-sensitive PMT [34]. PMT has two major undesired properties that make its integration in PET/MR systems indeed difficult. These are the sensitivity to magnetic field and the relatively large structure that impedes its easy integration inside the magnetic bore. Keeping the PMT tube at a distance from the magnetic field fringe below 500 μT has been reported in simultaneous preclinical PET/MR system. However, this configuration results in great reduction of scintillation light (90 %) leading to a degraded energy resolution [31].

9.3.5.2 Avalanche Photodiode (APD)

One of the major transitions in the field of PET/MR detector technology is the use of semiconductor photosensors in PET detector design [32]. APD operates below the breakdown voltage, and the signal produced is proportional to the ion pair created and to the energy deposited by the coincident photons interacted with the crystal. APDs also have an advantage over PMTs in not requiring high bias voltages to operate. At reverse bias, a volume close to the junction is depleted of

Table 9.2 Comparison of three major photodetectors used in clinical or preclinical PET/MR imaging systems[a]

Characteristic	PMT	APD	SiPM
Active area (mm^2)	1–2000 cm^2	1–100 mm^2	1–10 mm^3
Gain	10^5–10^7	100	10^5–10^7
Rise time	<1 ns	2–3 ns	~1 ns
Dark current/count rate	<0.1 nA/cm^2	1–10 nA/mm^2	0.1–1 MHz/mm^2
Capacitance (pF/mm^2)	9	2–10	>30
Quantum efficiency @ 420 nm (%)	25	60–80	<40[a] [~25–75] Photon detection efficiency
After pulsing	Yes	No	Yes
Bias voltage (V)	1000–2000	~200–1500	~50 [30–80]
Power consumption	100 mW/ch	10 μW/mm^2	<50 μW/mm^2
Temperature coefficient (%/°C)	<1 %/°C	2–3 %/°C	3–5 %/°C
Bias coefficient	<1 %/V	10 %/V	~100 %/V
Magnetic susceptibility	Very high (mT)	No (up to 9.4 T)	No (up to 15 T)
Price/channel ($) in 2010	>200	~100	~50

[a]Taken from [41, 44]

free charge carriers. The charge carriers created in the depleted region drift in the electric field toward corresponding electrodes and, while traversing this region, acquire enough energy to produce electron-hole pairs by impact ionization. The newly created charge carriers may create new ones and so on. Thus, there is an avalanche of electrons and holes moving through the detector. An external circuit then detects these current pulses [37].

The quantum efficiency reaches 70–80 %, and when coupled to LSO crystal (peak wavelength 420 nm), the timing resolution lies in the range of few nanosecond. Avalanche photodiodes provide great advantages in terms of dimension and subsequent detector design compactness. The small size provided by APD is a positive characteristic toward an improved spatial resolution that matches small crystal dimensions and high packing fraction. The insensitivity to magnetic field was central property that made APD an acceptable alternative to PMT in PET/MR systems [38]. APD coupled to LSO crystal in preclinical 9.4 T magnet showed stable performance with no dependence in gain and energy resolution (14.4 % at 511 keV) of APD on the magnetic field. There was also no effect of changes in the orientation of the APD electric field with respect to the main magnetic field lines (parallel vs. perpendicular), hence proving the feasibility of operating such a PET detector module inside an MRI [39].

However, APD has a number of limitations that requires special attention in the detector system. It has low internal gain (10^2–10^3) and requires charge-sensitive preamplifiers to convert electron charge to a measurable voltage signal. Charge integration occurs over several nanoseconds to achieve high conversion factors, and pulse pileup takes place at high counting rates. APD needs advanced front-end electronics to meet the lower gain, and therefore special and application-specific integrated circuits are used [40]. Noise and time variation in electron drift during multiplication process are factors that restrict using the APD in time of flight applications [41]. The gain is sensitive to changes in temperature and voltages applied, and thus special measures are required to control these technical factors. Thus, temperature sensitivity of APD imposes special constraint on the design of PET/MR such that a well control over the solid-state detector should be maintained and eddy current, if not minimized, would affect the gain of the electron avalanche due to increased collision with semiconductor lattice [36, 37]; see Table 9.2.

APD can be coupled directly to the scintillator but also can be located at a short distance

using optical fibers, depending in large part on system configuration including space allocated for PET module inside the magnet and minimizing the interference between the two subsystems [15, 42]. The advent of APD to the medical arena has been attractive for large academic institutions to build their own hybrid PET/MR systems. It has been successful in initial attempts made to construct simultaneous hybrid systems with further investigations performed to optimize the design and improve the quality of either systems [43]. The first insert-type PET detector was a prototype released by Siemens (BrainPET, Siemens Healthcare, Inc.) providing an opportunity to acquire a simultaneous PET/MR on human brain [17, 43] as mentioned earlier. The insert was integrated with a standard 3-T MRI scanner (Magnetom TIM Trio; Siemens Healthcare, Inc.), and proof-of-principle simultaneous data acquisition was demonstrated. In addition, the BrainPET can be docked at the back of the magnet without obstructing the bore so that the MR scanner can be used in standalone mode [17, 43].

9.3.5.3 Silicon Photomultiplier (SiPM)

Geiger-mode avalanche photodiode (AVP) or SiPM (also called multi-pixel photon counter) is made of arrays of small APD (e.g., 50 × 50 μm) and operated beyond the voltage breakdown in the Geiger counting mode [44]. The compact size permits also an easy incorporation in small animal PET/MR systems and implementation in depth of interaction-based scanners [31]. In this solid-state photodetector, the high electric field in a very small space that collects the ion pair allows for better quantum efficiency and provides good resistance to magnetic field in contrary to those effects seen in PMT. It was shown that SiPM can tolerate a magnetic field of 7 T [45]. Coupling of the SiPM to scintillation needs some attention especially one-to-one coupling as it increases the number of photodetector in the magnet substantially; however, it eliminates light sharing and improves spatial resolution [31, 41].

Like APD, low temperature is also an important prerequisite for operating SiPM, and variation in temperature can lead to alteration of the breakdown voltage and subsequent variation of photodetection efficiency, dark current, and gain [27]. Each cell in SiPM photodetector works independently, and the charge created from the ion pair is no longer proportional to the energy deposited, but the summed output from all cells is proportional to the energy deposited in the scintillator. It is therefore important to maintain good energy linearity as photodetector outputs need to be compared in crystal identification schemes [11]. While the quantum efficiency of APD is nearly 80 % (as mentioned above), the photodetection efficiency of SiPM is below 40 % when coupled to LSO crystal. Proper eddy current management, cooling system, and accounting for residual inaccuracies in system calibration are measures taken to tackle heat generation and associated problems.

Based on the above discussion, the SiPM has a high gain similar to that revealed from PMT, resistance to high magnetic field, and low bias voltage when compared to APD. The emerging digital SiPMs have shown improved performance and low temperature sensitivity. It also provides a good timing, energy and spatial resolution, as well as good temperature stability, making it a promising candidate concerning their MR compatibility. However, they tend to generate digital electromagnetic noise patterns which might degrade the MR image quality; a design measure that needs to be taken into consideration [46]. Table 9.1 compares the three commonly used photodetectors used in PET/MR.

As previously mentioned, the Signa PET/MR from GE Healthcare utilizes the SiPM technology. This new digital detector is characterized by its enhanced sensitivity; it is up to three times more sensitive than GE Healthcare's Discovery 690 PET/CT. SiPM photosensor is also being adopted in the European Hyperimage collaboration to build a small animal PET insert inside a clinical 3 T MR system of a ring diameter of 20 cm and axial field of view of 9 cm. Each detector comprises a 22 by 22 array of 1.3 × 1.3 × 10 mm^3 LYSO crystals coupled to an 8 × 8 array of 4 × 4 mm^2 SiPM where the signal is immediately digitized using application-specific integrated circuit (ASIC) that release digital energy,

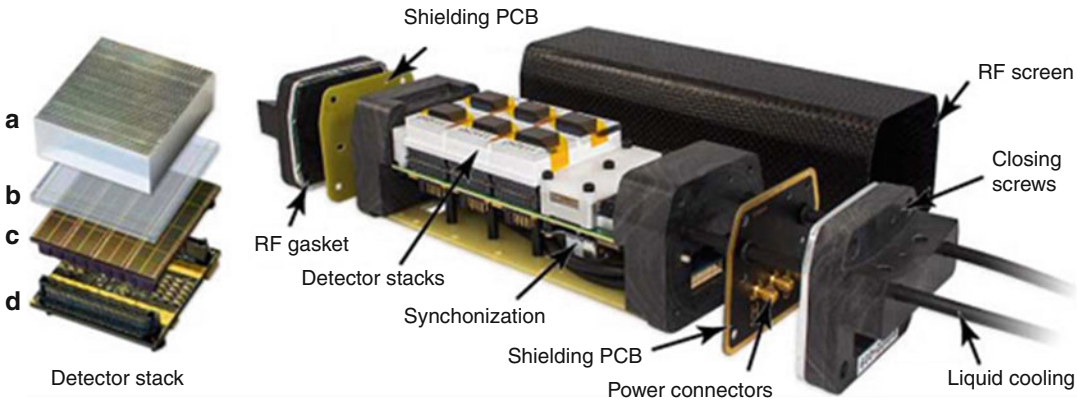

Fig. 9.5 Digital silicon photomultiplier (dSiPM)-based detector stack (*left*) with scintillation crystal array (**a**), light guide (**b**), sensor (**c**), and interface board (**d**). On the right side of the figure, the single detection module (SDM) contains up to six detector stacks. The carbon fiber shield is pushed over the module and the RF screen is closed on both sides by shielding plates (From Ref. [48] under Creative Commons Attribution 3.0 License)

timing, and channel information [46, 47]. This last feature is substantial as it reduces and could eliminate the interference that affects connection and transmission cables between photodetectors and signal processing circuitry. See Fig. 9.5.

9.4 MR System Technology

An MR imaging system has several major components that interplay to acquire an image. The most important parts are static magnetic field, gradient magnet, and radio-frequency coil. The magnetic field magnetizes the human body once the patient is inside the magnet bore. Most of the imaging interest in MR is the hydrogen atom (i.e., protons) due to its plenty and large abundance in human tissues and cells. Under the strong magnetic field applied by the static magnet, the protons are aligned into two directions: parallel and antiparallel. Majority of protons are aligned in parallel with the magnetic field (B_o) in comparison to those protons aligned antiparallel as the former is a lower energy state compared to high energy state of the antiparallel direction. A net magnetization is therefore produced in parallel to the magnetic field (B_o) and takes place along the z-direction. In addition, a precession or rotational motion of the protons is created that precess with frequency proportional to the magnetic field. In clinical setting, 1.5 and 3 T static magnet is used, but higher strength (e.g., 7 and 9.4 T) is used for more advanced application. It is important to maintain the homogeneity of the static magnetic field, and any component of magnetic susceptibility (a property of a material to be magnetic when exposed to magnetic field) must be avoided or adequately isolated within the field of view to keep image quality with minimal distortion.

The gradient coil has an important role in providing a spatial localization of the MR signal by varying the static field strength in the three orthogonal planes in a linear fashion. Gradients are loops of wire or thin conductive sheets on a cylindrical shell lying just inside the bore of an MR scanner. When current is passed through these coils, a secondary magnetic field is created. This *gradient field* slightly distorts the main magnetic field in a predictable pattern, causing the resonance frequency of protons to vary as a function of position. The primary function of gradients, therefore, is to allow a spatial encoding of the MR signal. Gradients are also critical for a wide range of "physiologic" techniques, such as MR angiography, diffusion, and perfusion imaging [49].

The second important part is the transmission coil which sends uniform radio-frequency excitation at the Larmor frequency over the field of view. Local receive coil or surface coil is placed over the region of interest to improve the magnetic sensitivity and hence signal-to-

noise ratio. This coil is also affected by distance such that the sensitivity decreases appreciably beyond a distance equal to the diameter of the coil. Upon relaxation and switching off the RF signal, the information received is processed using a reconstruction algorithm from 2D to 3D images of the resonance signal [27].

Most commercial MRI scanners are superconducting high-field strength magnets because of their faster scanning ability, higher magnetic field homogeneity, higher SNR, and wider range of applications. In a superconducting magnet, a magnetic field is generated by a current that runs through a loop of wire. The wire is surrounded with a coolant, such as liquid helium, to markedly reduce the electric resistance of the wire. Once a system is energized, it maintains its magnetic field [50]. Early work on PET/MR systems was specially focused on manufacturing an MR-compatible PET detector with modifications made to the PET detector system. Recent approaches taken are to modify aspects of the MRI in order to achieve close integration and minimize interactions between the two systems within the magnet bore [25].

9.4.1 Magnetic Shielding

The presence of PET front-end electronics and data transmission cables inside the magnet bore represents one of the major challenges in hybrid simultaneous PET/MR systems. A proper but effective shielding system should be implemented to reduce to an acceptable level the interferences that come from the gradient as well as radio-frequency pulse and able not to disturb the main magnetic field uniformity [51]. Signal reflection and absorption together with material skin depth are important physical measures of the shield. Moreover, magnetic susceptibility, gamma rays' attenuation coefficient, and eddy currents are factors to be considered in the candidate shield material. Connection and transmission cables need also a sort of attention as it needs to be masked from the above interferences sources.

Reflection loss is proportional to material conductivity and inversely proportional to permeability, while absorption loss is proportional to conductivity, permeability, and thickness of the shield [27]. In electromagnetism, permeability is the measure of the ability of a material to support the formation of a magnetic field within itself. Hence, it is the degree of magnetization that a material obtains in response to an applied magnetic field. Skin depth, however, is inversely proportional to permeability, electrical conductivity, and signal frequency. One skin depth is defined as the required thickness of a metal to reduce the RF to 37 % of its original strength. The smaller the skin depth, the thinner the material is used for shielding to a particular level. Gradient switching typical in MRI sequences can result in count losses in the particular PET detector design studied. Moreover, the magnitude of this effect depends on the location of the detector within the magnet bore and which MRI gradient is being switched. This information is substantial in the design of PET shielding in MR environment [43].

Aluminum (Al), copper (Cu), and carbon (C) are different materials that can be used for shielding. High conductive materials, e.g., copper, show excellent radio-frequency (RF) shielding properties, but have negative impact on the MRI image quality due to induced eddy currents. However, carbon fiber composites are less conductive for low frequencies and thus can minimize MRI gradient-induced eddy currents. Furthermore, they show good RF shielding properties for higher frequencies. First prototypes using carbon fiber have shown excellent eddy current performance, good RF shielding properties, and superior mechanical robustness in a preclinical simultaneous PET/MRI insert in a clinical 3-T scanner [52].

In a different setting of 7-T PET/MR preclinical scanner (RF at Larmor frequency of 300 MHz, 81 kHz from gradient power supply), placing the PET detector module between two carbon fiber tubes and grounding the inner carbon fiber tube to the PET detector module ground reduced the RF and the eddy currents. Further reductions were achieved by adding thin copper (Cu) foil on the outer carbon fiber case and electrically grounding the PET detector module so that all three components had a common ground [43].

9.5 Small Animal PET/MR

As outlined earlier, initial incentives on PET/MR imaging were on developing small animal hybrid system. This has several advantages in terms of superb soft tissue contrast provided by MRI and wide range of MRI sequences that address anatomical and functional questions in biomedical imaging research [53]. Radiation dose reduction is also another important advantage provided by PET/MR when compared to PET/CT due to the great reduction of cumulated radiation dose over several sessions as occurs in longitudinal studies. Small animal imaging has become a substantial tool in development of new diagnostic biomarkers and drug and essential step in translational medicine. Hybrid PET/MR should have a superb spatial and contrast resolution in order to meet small structure challenges posed by rodents such as mice and rats during in vivo animal imaging. In addition to the difficulties placed by the integration of the PET and MR scanners into one hybrid system, the spatial and temporal resolution together with system sensitivity should also be enhanced.

Small animal hybrid PET/MR systems vary substantially in terms of design parameters that include but not limited to magnet strength, scintillator-photodetector coupling method, type of photodetectors and associated electronics, arrangement of the front-end electronics, and configuration and positioning of the gradient and RF coils. Also, there are some variations in PET detector ring dimensions (axial and transaxial field of views), shielding of the PET electronics, and methods of reducing mutual interferences between the two subsystems. The PET detector is mostly LSO-based scintillator with different array size and segmentation and also whether it is positioned at distance or in direct coupling to readout photodetector.

The use of position-sensitive APD (PSAPD) has become attractive for some reasons such as less contact terminals and hence less connection lines. It consist of a continuous layer of detector material with output terminals positioned such that the relative intensity of the avalanche signal at these contacts serves to determine the exact location of the photon interaction [42]. This easily permits incorporation of PET system electronics within the magnet bore while maintaining the same spatial resolution provided by the conventional APD, as well as it helps reducing costs and complexity of system design. Depth of interaction or parallax error is a potential source of resolution degradation due to radial shift of radioactivity from detector center within the PET ring. The small solid angle and increased crystal thickness are desired detector properties in small animal PET systems but unfortunately serve to increase this parallax error that can be mitigated with the use of PSAPD [54].

Two nonstandard designs employed by different research groups are split magnet and field-cycled PET/MR systems. The former was devised and employed in Cambridge small animal PET/MR model in which the microPET Focus 120 was inserted in a gap of 80 mm between a split 1-T superconducting magnet (Fig. 9.6). The magnet and the PMT were appropriately shielded producing a net magnetic field below 1 mT around the PMT. Furthermore, the gradient was also split with little impact on static field homogeneity and gradient performance [55]. A novel set of gradient and shim coils has been specially designed for this split MRI scanner to include an 110-mm gap from which wires are excluded so as not to interfere with annihilation detection [55].

Field-cycled MRI systems use two independent, actively controlled resistive magnets to polarize a sample and to provide the magnetic field environment during data acquisition producing comparable quality to clinical superconducting systems [56]. The static magnet is split so that the PET block detectors can be placed but with less shielding to the detector and without the use of optical fibers. However, the gradient magnet is not split in this design [57].

Mediso nanoScan® PET/MRI scanner consists of PET scanner (LYSO coupled to 256 channel position-sensitive PMT) in sequential mode with 1 T static magnet [59]. The PET component of the instrument is based on the PET ring of the NanoPET/CT scanner [60]. The PET detector consists of 12 modules, each comprising a 39 × 81 (tangential x axial) array of 1.12 × 1.12 × 13.00 mm

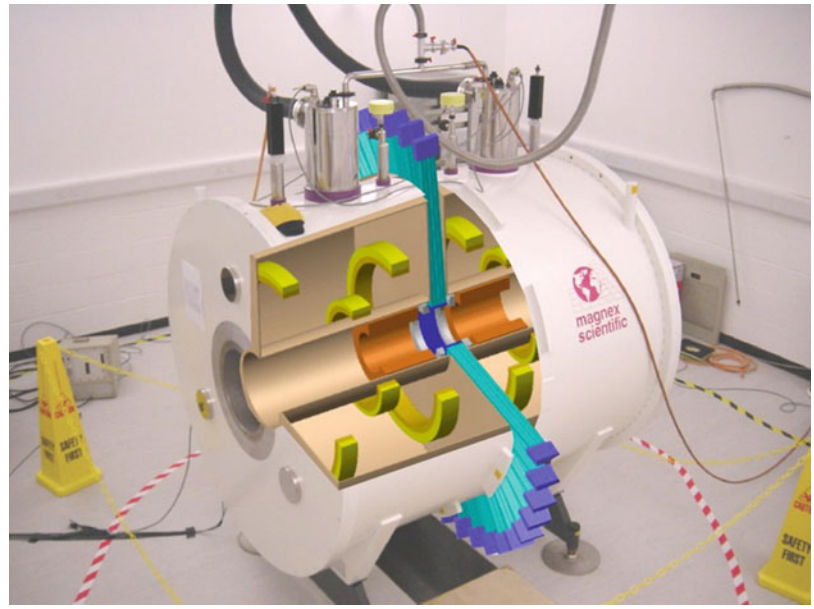

Fig. 9.6 The preclinical PET/MR Cambridge model where 1 T actively shielded superconducting magnet with 80-mm gap to accommodate a multi-ring PET detector array is shown. The PET detectors and MR imager view the same region in space, which facilitates simultaneous MRI and PET acquisition (Reprinted from Ref. [58] with permission)

LYSO crystal on a pitch of 1.17 mm, and the system matrix is monitored by two position-sensitive photomultipliers (PSPMT). The MR imaging component of the instrument is based on the M2 system by Aspect Imaging. The 1-T vertical field, horizontal-bore permanent magnet has better than 5-ppm homogeneity in the central 60-mm-diameter region and a fringe field below 13 mT anywhere on the magnet surface. It features built-in gradient coils used for shimming and an internal radio-frequency cage. The gradient can deliver 450 mT/m pulses with a 250-μs ramp time. It was shown that system integration had no adverse effect on the PET performance with acceptable system spatial resolution and sensitivity [59].

A recent report highlighting the use of digital SiPM coupled to LYSO assembled in MRI-compatible PET insert has been published [48]. Digital SiPM from Philips Digital Photon Counting (PDPC) was used to develop a preclinical PET/RF gantry as an insert for clinical MRI scanners. The scintillation arrays were made from 30×30 12-mm-long LYSO crystal applying 1-mm crystal pitch and optical isolation. With three exchangeable RF coils, the hybrid field of view has a maximum size of 160 × 96.6 mm (transaxial x axial). Depending on the coil, MRI SNR is decreased by 13 or 5% by the PET system. PET performance measures such as count rates, energy resolution (12.6% full width at half maximum, FWHM), and spatial resolution (0.73 mm^3) were not affected by applied MRI sequences. PET time resolution of 565 ps (FWHM) is degraded by 6 ps during an echo planar imaging [48]. See Fig. 9.7.

9.6 Attenuation Correction

Photon attenuation is the major source of errors in SPECT and PET imaging [61]. Photoelectric effect and Compton scattering are the two main interactions that serve to produce suboptimal quantitative results and deteriorated image quality. The former results in photon absorption and complete loss of the 511 keV photons energy, while the latter interaction serves to reduce photon energy by imparting part of the incident energy to the orbital electrons. When considering the total attenuation length that varies from small range as in patient skull or more longer as in chest area, there is approximately 5–22% of the PET signal that is recoded by the scanner accounting for attenuation factors of 18 and 4.5, respectively. These measures indicate that small errors or erroneous values may lead to a

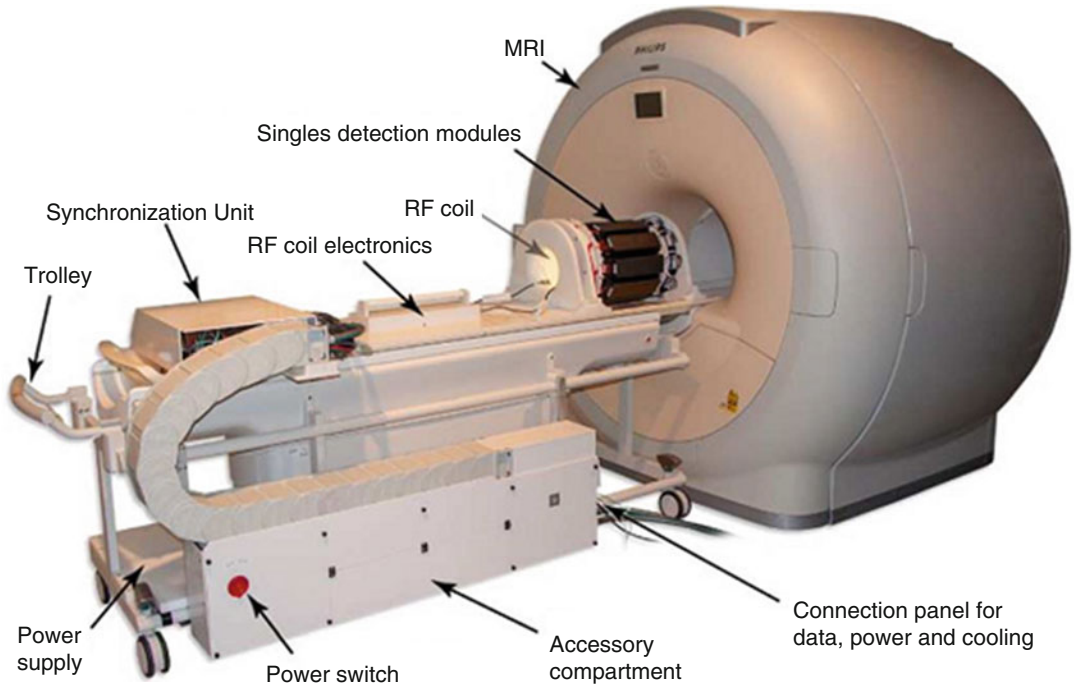

Fig. 9.7 The PET/RF insert "Hyperion II^D" mounted on the patient table of a clinical 3 T MRI system (gantry cover removed). The single detector module is described in Fig. 9.4 (Reprinted from Ref. [48] under Creative Commons Attribution 3.0 License)

significant deterioration of image quantitative accuracy [62].

The traditional way of attenuation correction in the past and still used in small percentage of old PET scanners is the use of radioactive transmission sources such as Cs-137 or Co-60 [63, 64]. After the advent of the PET/CT and introduction of the CT as complementary component in the diagnostic process, it has become so feasible to use the Hounsfield units to get the μ-values of individual image pixels. This permits to derive the attenuation correction factors by forward projecting the μ-map produced from the CT scan. Low dose, diagnostic, or contrast-enhanced CT images (with treatment of increased area of contrast concentration) can be used for CT-based attenuation correction using the most common method of bilinear transformation. In this algorithm, HU units below zero are considered as combination of water and air, while values above zero are considered as combination of the bone and soft tissue. This assumption allows one to produce a two regression lines intersecting at HU of zero with different regression slopes [65, 66]. However, two important steps need to be considered while correcting for photon attenuation in CT. The first is pixel down-sampling due to small size of the pixels of the CT image in comparison to PET image. The second is the energy conversion of the μ-values produced from the CT energy photons (around 50 keV for 120 kV tube voltage) to the corresponding value at 511 keV [65].

For the purpose of relative and absolute quantitative PET imaging, correction of photon attenuation is a fundamental prerequisite to achieve better image quality and acceptable quantitative accuracy. MRI data set, on the other hand, has an essential drawback in which the images reflect protons' density and longitudinal (T1) and transverse (T2) magnetization relaxation properties of the tissue of interest. These parameters unfortunately don't reflect the electron density and attenuation properties of the human tissues, and this is exemplified in bone- and air-containing tissues such as the skeletal system and lung tissues, respectively. Both tissues have similar MRI

signal output and greatly influence the correction process. Therefore, correction of photon attenuation in PET/MR is not a straightforward process, and some maneuvers are required to tackle this issue. Various approaches have been developed such as those based on templates, atlas information, direct segmentation of T1-weighted MR images, or segmentation of images from special MR sequences, as well as methods relying on PET emission data and MR anatomic information to obtain attenuation map [67].

9.6.1 Template-Based Attenuation Correction

In this technique, an MR template image and co-registered attenuation correction map are generated. The MR template can be produced from MR T1-weighted images and the attenuation map can be derived from transmission scan [68, 69]. The MR template is initially warped to fit the patient MR image using nonlinear registration, and the transformation parameters are used to align the attenuation map template to the PET data of the same patient. This process allows one to produce an individual attenuation map for a given patient study. The incorporation of bone tissues into the correction is relatively easy, but the algorithm suffers from misalignment errors caused by nonlinear registration due to inter-patient anatomical variations. Variants of this method include gender specific or combination of both male and female to generate attenuation map template or produce an average template based on spatial normalization of the individual MR images and the associated co-registered measured attenuation maps [70]. Template-based methods are common only in brain studies.

9.6.2 Atlas-Based Attenuation Correction

Atlas-based approaches are implemented using global anatomical knowledge derived from a representative intensity-based or segmented reference data set into the attenuation correction process. Atlas-based methods have been devised to account for bone attenuation in the PET/MR hybrid images using the bone tissue density revealed from co-registration with CT template [71]. The idea is to utilize a standard CT atlas or a combination of MR and CT atlas data sets and co-register with the patient MR data set to come up with information regarding the transformation parameters. This information is then used to produce a pseudo or synthetic CT data set valid for attenuation correction [67, 72].

One approach is to deform one representative CT data to co-register with patient MR image, and then the newly deformed CT is used for PET data attenuation correction. The registration is carried out through a multistep process that include rigid, B-spline, and optical flow [73]. Another approach utilizes a pair of CT and MR atlas to produce the pseudo-CT data set. In this algorithm, the MR atlas is co-registered with the patient MR, and the transformation parameters are then applied to the CT atlas to produce individualized CT attenuation map. The pseudo-CT data set is weighted sum from each co-registered atlas data set [71, 74].

Advantages of atlas-based methods are the possibility of providing attenuation maps with continuous linear attenuation coefficients eliminating issues associated with the use of single tissue values that do not account for tissue heterogeneities [75]. However, shortcomings of these algorithms include limitations in identifying pathologic lesion using the atlas data set, lung density variations among different patients, and metallic implants. Performance of atlas-based algorithms can be enhanced by the incorporation of the pattern recognition, multiple sequences to improve tissue classification, modifying the registrations method, and artifact detection [71, 76–79].

A relatively recent study compared four different methods in MR attenuation correction in relation to CT-based attenuation correction [76]. Namely:

1. Two segmentation-based methods that do not account for the bone.
2. An atlas and pattern recognition method and accounted for the bone.

3. A hybrid method that combined both approaches, atlas-based and segmentation. It accounted for the bone tissues such that the attenuation map in areas where the bone is likely to occur was predicted with atlas and pattern recognition, whereas a segmentation-based method was used for the rest of the body.

For soft tissue lesions, none of the methods revealed a significant difference, whereas for bone lesions, underestimation of PET standardized uptake values was found for all methods with minimized error for the atlas-based approaches. There were also underestimations of lower magnitude observed in lesions near to bony structure. For lesions affected by MR susceptibility artifacts, quantification errors could be reduced using the atlas-based artifact correction [76].

9.6.3 Image Segmentation

Image segmentation is the process of classifying or clustering every similar group of pixels into a distinct category. In MR segmentation, image intensity is the most common way that enables to classify the human body into air, water, and fats. However and as mentioned earlier, areas that contain air or bone structures have poor MR signal and thus imposing great difficulties on segmentation and classification algorithms. The algorithm works such that every group of pixels that have the same MR signal would be assigned the same tissue properties and hence will be given corresponding attenuation coefficients.

Direct segmentation methods depend on MR T1-weighted sequence routinely acquired in patient examinations. Segmentation methods have been applied to brain as well as whole-body PET/MR imaging procedures. Approaches like the use of fuzzy clustering and anatomical knowledge combined with neural network-based tissue classification have been reported. These methods require further processing tools to segment, for example, lung tissues, bone structures, or outlining the body boundaries [80–84].

Specific MR sequences combined with segmentation algorithms are the most common approach employed in clinical practice of attenuation correction in PET/MR imaging systems [75]. It is based on the two-point Dixon gradient echo sequence that enables separation of water and fat tissues by using the chemical shift of fat relative to that of water. This allows one to segment the MR images into individual different tissue types including either 3-class (air, lung, soft tissue) or 4-class segmentation (air, lung, soft tissue, and fat). The former has no distinction between water-equivalent and fat tissues, while the latter provides water and fat distinction using Dixon MRI sequence [81, 83, 85, 86]. Figure 9.8 shows the attenuation map derived from different methods.

One major drawback of image segmentation using this approach is that every individual tissue is given a specific value ignoring tissue heterogeneities. Another drawback is the absence of bone signal, and its similarity to air-containing structures serves to confound the attenuation correction process. The deviation of the quantitative results relies on the location of the pathology and areas of osseous lesions [82, 84].

It is not only the location and type of tissues but quantitative results could also be negatively impacted by the composition of the bone lesions. An underestimation of more than 20 % of tracer concentration was found in the brain cortex when inaccurate assessment of bone attenuation was performed while not identifying the internal cavities resulted in more than 20 % overestimation of the adjacent structures [87]. In the same report, ignoring the RF coil in the attenuation correction process leads to up to 50 % underestimation of the reconstructed PET images.

In whole body, the situation is relatively different as bone segmentation is not so influential, especially in body regions located at distance from bone tissues, as in brain-based applications. There were some directions to perform segmentation without bone classification in areas of the body that are not adjacent to bone structure without a trade-off in quantification accuracy or image interpretation [83]. Another issue is lung segmentation which appears with low signal in conventional MR sequences in addition to inter-patient variability in tissue density. The utilization of

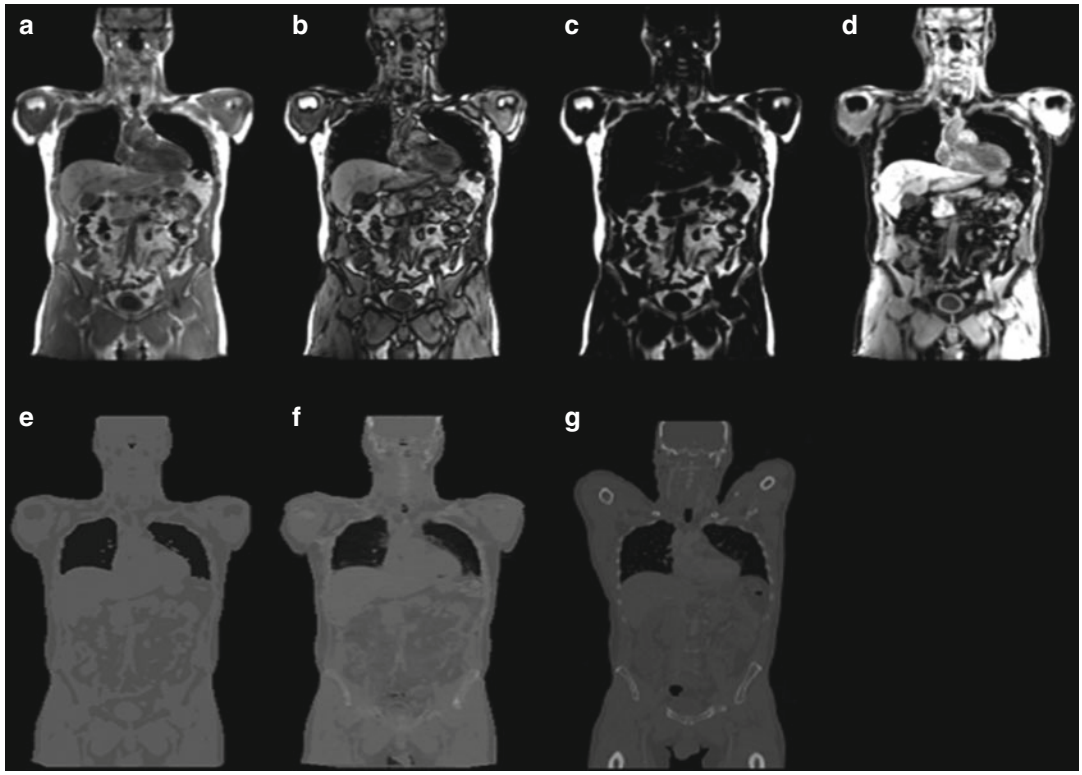

Fig. 9.8 Upper row: a sample MR data set acquired with a T1-weighted 3D gradient echo sequence with 2-point Dixon fat and water separation. (**a**) In-phase, (**b**) opposed phase, (**c**) fat, and (**d**) water images. Lower row: attenuation maps created from the MR data using (**e**) the segmentation method based on Martinez-Möller [83] and (**f**) the atlas- and pattern recognition-based method described in Hofmann et al. [71]. (**g**) The corresponding CT slice from the same patient (Reproduced from Ref. [88] with permission)

ultrashort echo time (UTE) or zero echo time (ZTE) sequences may benefit this problem by preserving signal within the lung parenchyma and therefore allows better differentiation of diseased or consolidated lung with possible incorporation of these values into tissue classifications [89]. The latter sequence was successfully implemented in skull attenuation correction when compared to corrections derived from CT data. The segmentation results show better bone depiction and separation from air cavities and collagenous tissue than previously reported methods; however, further work would be interesting to show its feasibility in chest and cardiac imaging [86].

The UTE sequence enables an improved signal of the bone tissue due to the low T2 relaxation times of the bone. This when combined with an image of longer echo time where bone signal is significantly low can produce an improved segmentation outcome of bone structures. Recently, this approach has been adopted to synthesize a brain CT image (or μ-map) from dual echo UTE images using reference or training data while avoiding the step of co-registering the reference atlas with the subject MR [90]. This algorithm (GENErative Sub-Image Synthesis, GENESIS) matches patches between the reference images and subject images based on a statistical model. It has three major features which are as follows: (1) it does not require any segmentation of the MR images, (2) it does not require the reference images to be registered to the subject images, and (3) it utilizes the MR images to determine the optimal matching patches in the reference data as well as the reference CT image [90].

UTE time sequences have also some limitations like increased acquisition time and induced artifacts when the field of view is increased. In

whole-body PET/MR, it will be time-consuming to use UTE. An underestimation down to 40 % and overestimation up to 11 % were recorded in brain PET quantitation using UTE sequence when compared to CT-based attenuation correction at the same location [91, 92]. Further improvement of UTE in clinically adopted PET/MR system has been suggested due in part to bone misclassification and in adequate performance in the neck and nasal/face area [93].

Joint estimation of radioactivity and attenuation from the emission data using a constrained maximum likelihood reconstruction of attenuation and activity has been also proposed to determine the attenuation map which improves by the inclusion of time of flight information [94]. Time of flight capabilities were found to improve the accuracy of attenuation correction especially when attenuation correction is not accurate [25, 95].

9.7 Data Acquisition

PET/MR imaging systems vary in their approach in data acquisition. Image acquisition may start by acquiring a short sequence for anatomical referencing and attenuation correction. Oncologic application is generally lengthier than non-oncologic studies and may extend to 60 or 70 min in simultaneous data acquisition. However, in sequential PET/MR examinations, the scan length may go up to 90 min [96]. PET data acquisition is simple in comparison to MRI since the former is a time-based acquisition system, and once the collected information is thought to satisfy the diagnostic task, nothing needs to be added. MRI sequences are various but longer and reveal different information and often the primary cause of prolonging the acquisition time.

Before starting looking at the appropriate protocol for a given patient study, a number of steps need to be taken into consideration. Patient preparation, instructions, positioning, and setup are some of those that should be viewed not only from one modality perspective but also from other diagnostic angles. In PET, physiologic parameters such as glucose levels or other safety concerns that are related to pregnancy or pediatric examinations will need to be properly assessed. In MR, some precautions need to be checked as well like metallic implants and patient claustrophobia, while patient motion remains an issue in both imaging techniques. Patient centering on the couch and positioning of the surface coils in addition to time taken to perform these tasks are important parameters to avoid imaging artifacts and reduce technologist radiation exposure [97]. Patient preparation in PET/MR studies shouldn't be different in terms of plasma glucose level, fasting conditions, hydration, pregnancy, and uptake period void of any muscular activity that also need to be potentially minimized 24 h before the commence of the study. MR patient precautions are different and include MR-incompatible implants and contraindications from injecting contrast agents.

9.7.1 Imaging Workflow

Imaging workflow is an essential element in the diagnostic workup and of considerable interest in patient throughput. It is controlled and managed through a number of variables such as the organ or disease under investigation, type of hybrid PET/MR scanner, patient indications, partial or whole-body scan, and other imaging logistics [12, 96, 97].

Workflow is platform dependent. Simultaneous systems provide about 10–15-min saving due to the fact that patient is positioned and removed only once [98]. Apart from acquisition time reduction, patient comfort, and other logistics, the clinical rationale behind simultaneous PET/MR needs to be fully exploited and demonstrated similar to its biomedical applications where several biological or physiological questions can be answered. However, one of the major goals is to maintain the total acquisition time as low as possible while achieving the required diagnostic accuracy. Another feature provided by simultaneous hybrid PET/MR is the ability of acquiring complex imaging workflow and multiple MR sequence acquisitions with different contrasts during the PET data acquisition [7, 8].

In cardiac and neurologic applications, one-bed position might be sufficient to address a particular clinical question, and the total acquisition time is

determined by the modality that would stay longer. Multiple bed positions might be needed, and this largely depends on scanner axial extent and the organ or disease under examination.

In oncology-based studies, the imaging protocol might differ significantly as different parts of the body may require different MR sequences and accordingly different time frames. For the same purpose, the acquisition time may be extended longer due to more elaborate examinations required such as those used in advanced molecular imaging applications and MR spectroscopy analysis [8]. Similar to stand-alone MR scanner, surface coils in PET/MR are used to increase MRI image quality and reduce imaging time. However, because the surface coils may cause additional photon attenuation of the 511-keV photons, only dedicated coils approved for PET/MRI should be used [8, 96].

In the trimodality imaging systems proposed by GE Healthcare as well as in tandem-based hybrid PET/MR introduced by Philips Company, imaging session can start in the MR module at approximately 25 min postinjection, and this permits to exploit the rest of the uptake time (around 30–35 min, usually 60 min uptake time) in performing the required MR sequences. Once the MR examination is carried out, then the patient can be moved to the PET/CT or PET portion of the imaging scanner [12, 13].

Whole-body PET/MR imaging protocol is significantly different than other organ-based protocols such as cardiac or neurological disorders. A scout or topogram initial image is performed outlining the axial extent of the patient under examination. This MR localizer is similar to the CT scout image normally taken in commencing PET/CT imaging procedures. The acquisition of PET data is taken in a step-and-shoot mode with bed acquisition time of 2–5 min, but it may extend for longer exploiting the time demanding feature of MR sequences [96]. Time of flight helps reduce the acquisition time or the injected dose further, but overall the acquisition time of PET is determined based on many factors such as clinical preferences and experience, system performance, and the adopted standard protocol [22].

In integrated PET/MR, the attenuation correction 2-point Dixon volume-interpolated breath-hold examination (VIBE) is performed first before the desired MR protocol for each bed position; VIBE takes 19 s. This is followed by the simultaneous acquisition of the PET and the desired MR sequence [99]. A number of diagnostic MRI sequences may be variably and flexibly selected based on body region and clinical indications but usually at a minimum include a T1-weighted and a T2-weighted sequence [97]. After completion of a whole-body scan, a dedicated MR imaging confined to one-bed position is started with or without simultaneous PET data acquisition. The dedicated MR imaging includes standard anatomic sequences and multiparametric MR sequences such as diffusion-weighted imaging (DWI), perfusion-weighted imaging (PWI), and dynamic contrast-enhanced (DCE) MR sequences, depending on the diagnostic purposes [18, 96].

In a similar fashion, in sequential design adopted by Philips Company, a specific MR sequence (i.e., MRAC) is run prior to PET acquisition. The MRAC sequence is acquired only with the integrated body coil of the MR scanner, matches the PET dimensions, and allows both anatomical detail and attenuation correction. The MRAC image is then segmented into three tissue classes (air, soft tissue, and lungs), and predetermined linear attenuation coefficients are assigned to each class (0, 0.095 and 0.022 cm^{-1}, respectively). An attenuation template of the patient table and MR coils (provided by system manufacturer) is incorporated into the attenuation correction map [100, 101].

To show data acquisition and imaging workflow provided in sequential PET/MR systems, one approach is to perform all the diagnostic MR acquisitions at the beginning, followed by attenuation correction dedicated sequences and then starting PET. For instance, this imaging scenario could be an indication to assess response to treatment or in head and neck cancer surgery planning [12, 50]. The acquisition time of MR sequences has been an issue as it works against patient comfort and low throughput imaging rate and is vulnerable to imaging artifacts due to likelihood of patient motion. New technologies are attempting to tackle this issue by developing fast pulse sequence in addition to parallel acquisition with

multiple coil elements and also the use of parallel transmission [44].

9.7.2 Motion in PET/MR

Object motion in photography is generally an undesired feature that results in image blurring but in medical imaging is a crucial source of image quality degradation and impaired quantitative accuracy. Patient motions either voluntary or involuntary are among those degrading sources that need special attention in routine clinical practice. Consequences are loss of sharp edges and difficulties in outlining pathologic lesions in addition to less confidence in image interpretation [56, 102].

This resulting image blurring is simply due to the lack of timing information about the moving object in relation to stationary assumptions of the detection process or absence of an accurate motion model in the iterative reconstruction scheme. Patient motion and associated imaging artifacts in PET/CT are discussed in details in Chap. 16. Although the scanning period of MR sequences is relatively lengthy and might appear that it could be in temporal matching with those images from PET scanning, the data acquired with time-averaging process by MR are not comparable to the same average process in PET data acquisition [11]. However, the MR data which are used for attenuation correction produce an image from an average of fewer respiratory cycles but carrying a lot of motion compared to CT.

Voluntary (cardiac and respiratory) and involuntary motion artifacts need to be addressed before an accurate image interpretation takes place. Organ or lesion motion causes a count smearing effect over an area larger than the actual size of the lesion and hence causes volume inaccuracy determination and loss of quantitative accuracy. Acquiring the images at small time interval using the conventional "freezing" or gating approach has been effective in eliminating many of the motion-related diagnostic artifacts, but still suffers from low sensitivity and high image noise with low statistical quality due to the short scan time. In case of static cardiac imaging and free-breathing conditions, the heart moves in the range of 4.9–9 mm due to heartbeat and respiration, together with changes in myocardial shape and density. ECG gating, however, helps to acquire multiple frames representing heart motion intervals from diastole to systole, and hence motion-related artifacts can be removed.

In an attempt to match the two data sets and improve attenuation correction in cardiac PET/MR, a specific pulse sequence (two-dimensional fast spoiled gradient-recalled echo (SPGR)) has been applied to obtain an average MR image of patient under free-breathing conditions [103]. MR images were converted into PET attenuation maps using a three-class tissue segmentation method. In the myocardium, the voxel-by-voxel differences and the differences in mean slice activity between the attenuation MR-corrected PET data and the average CT-corrected PET data were found to be small (less than 7 %). The use of MR-derived attenuation images in place of CT-based attenuation correction did not also affect the summed stress score [103].

In principle, an accurate attenuation correction map is obtained if the CT- or MR-derived attenuation coefficients have the same static or dynamic phase as the acquired PET data. Diaphragmatic motion (i.e., 7–28 mm excursion) is a major source of image spatial resolution loss and degraded quantitative accuracy such as SUV measurements. It is of particular importance in oncological studies where the lung and upper abdomen are involved in a number of different tumor types. In similar fashion to cardiac gating, the respiratory signal can be acquired over short time bins (i.e., respiratory gating), and this approach was found successful in part solving motion-associated artifacts. It also prolongs the acquisition time affecting patient comfort and reduce patient throughput. Nevertheless, gating methods are the most widely used in motion correction strategies in the clinic. Realignment of the PET image bins after reconstruction into a single reference image is also a proposed solution but denatures the Poisson characteristics of the PET data [104, 105].

Using the list-mode PET data to derive motion estimates based on elastic deformation from simulated respiratory gating phantom has been proposed [106, 107]. Comparison of corrected and uncorrected respiratory motion average frames

suggests that an affine transformation in the list-mode data prior to reconstruction can produce significant improvements in accounting for respiratory motion artifacts in the lungs and heart [104]. On the other hand, list-mode-based and model-based image reconstruction where motion information is incorporated, similar to other image-degrading factors, in the framework of image reconstruction has shown to be superior in improving the temporal sampling as well as a reduction in the effects of irregular respiratory motion [106, 108].

The simultaneous nature of some hybrid PET/MR opened new avenues for researchers to use the MRI information to address the issue of organ motion by either using simple methods such as T2-weighted imaging during free breathing and T1-weighted imaging using either shallow end expiration or free breathing using a radial acquisition scheme [105, 109]. More advanced approaches are to use motion-sensitive MRI imaging sequences such as velocity-encoded phase contrast MRI (VEPC-MRI) or MRI tagging technique [105, 110]. MRI-based motion correction has not demonstrated robust translation into the clinic because of signal to noise and/or field of view problems within the larger human. The most promising techniques proposed with human applications include a T1-weighted approach that utilizes navigator echoes combined with either a 2D multi-slice gradient echo technique [111] or a steady-state free precession (SSFP) [104] in order to both track the respiratory excursion and create a motion tracking field that is utilized in the PET processing algorithm [109].

Tagged MR uses a special pulse sequence to create temporary features (tags) in tissue, which deform and can be tracked in images as the anatomy deforms. Another recent approach has been devised such that no external hardware exist to provide a respiratory signal and no change to the imaging examination except for the addition of a short PET/MR sequence after the clinical acquisition [112]. The authors hypothesized that sufficient data for respiratory correction can be acquired in just 1 min. The acquisition was used to build a patient-specific respiratory motion model and then used to motion correct the clinical PET data of any duration. The method used only standard MR sequences and image registration techniques. The PET-derived signal was used to drive a motion model formed by nonrigid registration of MR slices acquired rapidly after the main scan. This motion was then incorporated into the PET reconstruction. An increase in SUV measurements has been reported, and sharpness of count profiles drawn over some lesions was observed. However, further work is requested to investigate the technical feasibility in clinical setting and to prove significant lesion detectability over large patient population [112].

An MR self-gating method was also applied to perform respiratory gating of the MRI data and simultaneously acquired PET raw data [113]. The MRI sequence allows for retrospective self-gating without the need for additional MRI navigator echoes or sensors attached to the patient. After gated PET reconstruction, the MRI motion model is used to fuse the individual gates into a single, motion-compensated volume with high SNR. The MRI motion model is utilized for motion-corrected PET image reconstruction according to the post-reconstruction registration scheme [113]. The motion model yielded a reduced motion blur and improved quantification accuracy compared to static reconstructions and in higher SNR compared to conventional gated reconstructions.

Figure 9.9 shows PET data acquired in a simultaneous mode with MR signal integrating motion correction, attenuation correction, and point spread function modeling into a single PET reconstruction framework. A dedicated MRI pulse sequence (denoted "NAV-TrueFISP") was used allowing an accurate measurement of respiratory motion in the lower abdomen. It is composed of two-dimensional (2D) multi-slice steady-state free precession MRI acquisitions ("TrueFISP") interleaved by pencil-beam navigator echoes.

9.8 Opportunities, Challenges, and Future

PET/MR provides a significant number of technical and clinical advantages to the current state of molecular and morphologic imaging. These features can be exploited to improve the overall perfor-

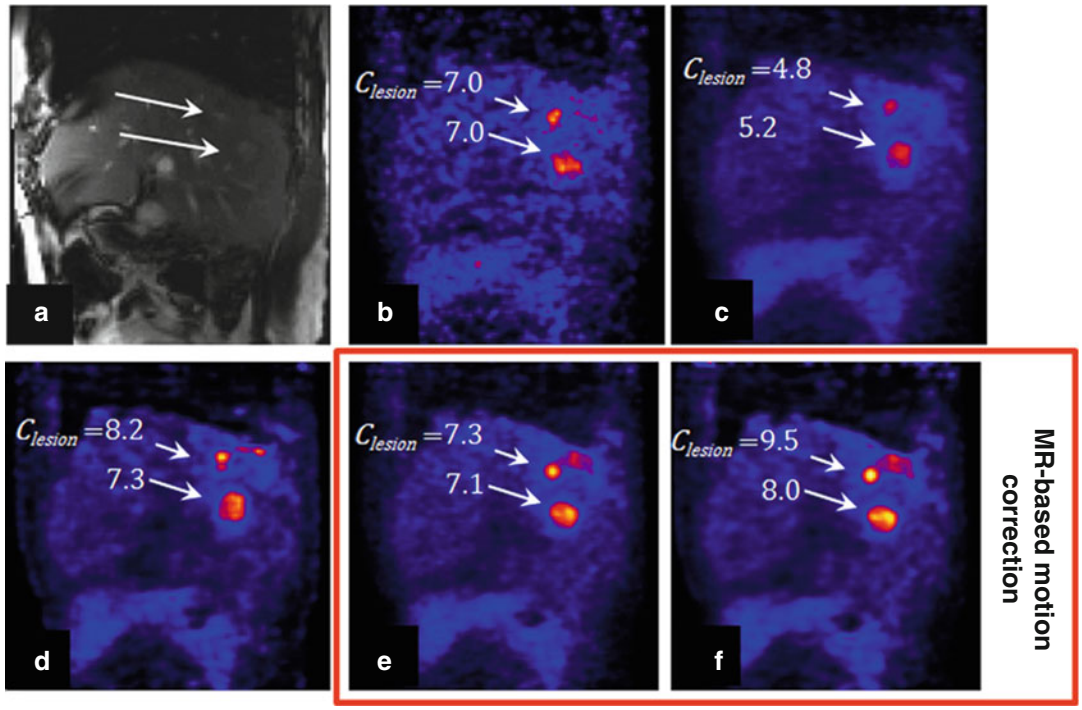

Fig. 9.9 Sagittal MRI (**a**) and corresponding PET slices reconstructed using (**b**) respiratory gating (OP-OSEM "gated"), (**c**) no motion correction (OP-OSEM), (**d**) no motion correction with PSF modeling (PSF-OP-OSEM), (**e**) MR-based motion correction (MC-OP-OSEM), and (**f**) motion and PSF corrections ("MC-PSF-OP-OSEM"). The gated volume was reconstructed using PET counts detected at end exhalation (approximately one-seventh of the total number of events). As can be seen, the proposed reconstruction methods (**e**, **f**) substantially improved hepatic lesion contrast and structure delineation as compared to the conventional uncorrected reconstruction method (**c**). *OP-OSEM* ordinary Poisson ordered-subset expectation, maximization, *PSF* point spread function (Reprinted from Ref. [114] with permission)

mance of hybrid PET/MR imaging systems in patient diagnosis, therapy, and management. The well-known improved soft tissue contrast characterizing MR imaging is a unique feature when compared to CT-based examinations. This characteristic is essential in brain studies, head and neck, abdomen, pelvis, and other soft tissue abnormalities. Furthermore, it will be beneficial in breast, liver, musculoskeletal, and urogenital imaging [115]. The lack of ionizing radiation in image acquisition is also an important asset in pediatric age group, pregnant women, and repeated acquisitions in patient follow-up and therapy monitoring. A recent work looking at diagnostic risk of medical exposure to CT scans in pediatric patients showed a probable triple risk of leukemia after a cumulative CT dose of 50 milligray (mGy), and a dose of 60 mGy might nearly triple the risk of brain tumors [116].

The simultaneous hybrid PET/MR imaging would in principle maximize the amount of information for real and direct benefit to patient management. MR can be very instrumental in synergizing the quality and quantitative accuracy of PET in terms of using the MR as guide to image reconstruction and incorporation of partial volume and/or attenuation correction in time of flight PET/MR systems [117–120]. MR-based motion correction and derivation of arterial input function are also potential applications that undergo significant research interest. Accurate determination of arterial input function is essential to obtain accurate physiologic parameter estimation when attempts are made to quantify tracer kinetics in absolute fashion. The MR component can help provide a way to determine blood flows such that partial volume correction and blood

vessel contribution to PET signal can be accounted for in the kinetic model. Realizing this last benefit would enhance the dynamic PET applications in routine practice in addition to eliminating the complications associated with arterial catheterization and serial blood sampling [121, 122].

In addition to superior contrast resolution among different types of soft tissue, MRI allows physiological (e.g., dynamic contrast-enhanced MRI), metabolic (e.g., MR spectroscopy), and molecular (e.g., diffusion-weighted imaging) besides functional MRI (fMRI) phenomena to be observed [123, 124]. MRI has a multitude of image pulse sequence that can flourish the diagnostic process, and when combined with PET data, particularly when using newly developed specific tracers, the amount of diagnostic information would be enormous and very supportive in clinical decision-making. For example, tumor perfusion using blood-oxygen-level-dependent (BOLD) imaging and correlating the results with O15-water or hypoxia-based tracers could substantially enhance the diagnostic interpretation [16, 125, 126]. Furthermore, the study of tumor uptake and dynamics with dual-labeled or more functionalized nanoparticle contrast agents and simultaneous PET/MRI monitoring of disease pharmacokinetics or pharmacodynamics are new avenues utilizing this multimodality imaging system [127].

PET/MR proved useful in a number of malignancies such as head and neck where improved soft tissue contrast is required. This can be represented by providing information about tumor extent and involvement of bony structures and bone marrow. Tissue reactions such as distortion, scarring, and fibrosis that appear posttreatment surveillance can obscure early detection of recurrence by conventional follow-up [128, 129]. It has also potential in evaluating pelvic malignancies such as gynecologic, rectal, and prostatic cancers because of its improved soft tissue discrimination compared with CT [130]. In breast imaging, specific breast MRI sequences permit high diagnostic accuracy for local tumor staging, and whole-body MRI can also be of great use in distant staging, especially when combined with F18-FDG-PET which has a high diagnostic performance for the detection of distant metastases [131]. FDG-PET/MR has an evolving role in breast cancer management, for example, in the detection of liver metastases and in the research setting for treatment monitoring [132].

In malignancies involving liver disease where metastases can occur from different sites, MR imaging has good diagnostic performance for lesions smaller than <10 mm; however, FDG-PET has some limitation such as heterogeneous uptake in the normal liver, its low sensitivity to lesions smaller than 10 mm, and the concomitant decrease in sensitivity in patients with underlying liver disease, including cirrhosis and nonalcoholic fatty liver disease [133, 134]. In bone marrow imaging, whole-body MR imaging has been proposed for detecting infiltrative focal bone marrow lesions and was demonstrated to have higher sensitivity than a skeletal survey for this task. It can also have potential in therapy monitoring or in the development of new therapies [129].

The role of PET/MR in neurology and psychiatry is one of the motivating aspects for developing such kind of devices due to the long-term experience of PET methodology and tracers in studying brain biochemistry. This has included a number of critical disorders that require early detection and response monitoring and even go beyond to stratify drugs in early stage of development. Anatomical and functional MRI information when combined with PET would have a definite incremental value to the diagnostic process in brain studies [135, 136]. In neuro-oncology, while gadolinium-enhanced MRI remains standard of care for brain tumor management (i.e., diagnosis, treatment, and posttreatment response assessment), other advanced MR techniques could be valuable in difficult cases providing key pathways into improved diagnostics. Different PET tracers such as F18-FLT, F18-FMISO, C11-Met, F18-FDOPA, and F18-FET can also assist in characterizing different aspects of tumor biology, and the availability of simultaneous PET/MR would facilitate investigations that look at improved patient management [135–137].

In cardiovascular diseases, PET imaging has unique capabilities in quantifying myocardial blood flow and flow reserve and is considered the

gold standard for assessing myocardial viability [see Chap. 19 for further details]. MR can be used to assess ventricle function, structural changes, perfusion, and tissue viability. It can also evaluate cardiac anatomy and detailed tissue characterization. Functional MR images and dynamic assessment of myocardial perfusion from transit of intravascular contrast medium can provide useful criteria for identifying areas of decreased myocardial perfusion or for assessing tissue viability from late contrast enhancement of scar tissue [138].

High temporal resolution cine image sequences have been devised to capture high-resolution images of the cardiac cycle. Blood flow can be visualized and measured via velocity-encoded cine sequences. Spectroscopic techniques, T1 mapping, and sequences capable of measuring myocardial strain are advanced MR techniques that can be integrated in the diagnostic scheme. Other utilities can be seen in detection of inflammation and characterizing atherosclerotic plaques and differentiate with a high risk of rupture from stable plaques. With the development of new tracers, there will be good opportunities in evaluating myocardial remodeling and in assessing the kinetics of stem cell therapy in myocardial infarction. New tracers will also provide new means for evaluating alterations in cardiac innervation, angiogenesis, and even the assessment of reporter gene technologies [138, 139].

Multimodal hybrid imaging in general and PET/MR in particular provide a great opportunity for understanding tumor pathophysiology and tackling biomedical questions that may arise from diagnostic or treatment clinical practices. The wide range of responses among patients suggests that further studies of individual responses to therapy, correlating structural and functional imaging, metabolic imaging, and clinical findings, will not only be helpful in understanding the mechanism of action of novel therapeutic agents but also support the new trend of precision medicine [129]. PET/MR could help in this dilemma by providing a one-stop-shop hybrid imaging platform that would eventually improve patient diagnosis and treatment outcomes. Extensive work has been and is being performed to elicit the several advantages of these systems in order to build up significant amount of evidences able to locate the hybrid PET/MR into its real clinical position in the near future.

References

1. Phelps ME. PET: the merging of biology and imaging into molecular imaging. J Nucl Med. 2000;41:661–81.
2. Chatziioannou AF. Molecular imaging of small animals with dedicated PET tomographs. Eur J Nucl Med Mol Imaging. 2002;29:98–114.
3. Jones T. Molecular imaging with PET – the future challenges. Br J Radiol. 2002;75:S6–15.
4. Yeh SH, Lin CF, Kong FL, et al. Molecular imaging of nonsmall cell lung carcinomas expressing active mutant EGFR kinase using PET with [(124)i]-morpholino-IPQA. Biomed Res Int. 2013;2013:549359.
5. Hammer BE, Christensen NL, Heil BG. Use of a magnetic field to increase the spatial resolution of positron emission tomography. Med Phys. 1994;21:1917–20.
6. Gaertner FC, Furst S, Schwaiger M. PET/MR: a paradigm shift. Cancer Imaging. 2013;13:36–52.
7. Jadvar H, Colletti PM. Competitive advantage of PET/MRI. Eur J Radiol. 2013;83:84–94.
8. Martinez-Moller A, Eiber M, Nekolla SG, et al. Workflow and scan protocol considerations for integrated whole-body PET/MRI in oncology. J Nucl Med. 2012;53:1415–26.
9. Beyer T, Townsend DW, Brun T, et al. A combined PET/CT scanner for clinical oncology. J Nucl Med. 2000;41:1369–79.
10. Townsend DW. Combined positron emission tomography-computed tomography: the historical perspective. Semin Ultrasound CT MR. 2008;29:232–5.
11. Zaidi H, Del Guerra A. An outlook on future design of hybrid PET/MRI systems. Med Phys. 2011;38:5667–89.
12. Kalemis A, Delattre BM, Heinzer S. Sequential whole-body PET/MR scanner: concept, clinical use, and optimisation after two years in the clinic. The manufacturer's perspective. MAGMA. 2012;26:5–23.
13. Veit-Haibach P, Kuhn FP, Wiesinger F, Delso G, von Schulthess G. PET-MR imaging using a tri-modality PET/CT-MR system with a dedicated shuttle in clinical routine. MAGMA. 2012;26:25–35.
14. Delso G, Furst S, Jakoby B, et al. Performance measurements of the Siemens mMR integrated whole-body PET/MR scanner. J Nucl Med. 2015;52:1914–22.
15. Judenhofer MS, Catana C, Swann BK, et al. PET/MR images acquired with a compact MR-compatible PET detector in a 7-T magnet. Radiology. 2007;244:807–14.
16. Judenhofer MS, Wehrl HF, Newport DF, et al. Simultaneous PET-MRI: a new approach for functional

and morphological imaging. Nat Med. 2008; 14:459–65.
17. Schlemmer HP, Pichler BJ, Schmand M, et al. Simultaneous MR/PET imaging of the human brain: feasibility study. Radiology. 2008;248:1028–35.
18. Yoo HJ, Lee JS, Lee JM. Integrated whole body MR/PET: where are we? Korean J Radiol. 2015;16:32–49.
19. Hawkes RC, Fryer TD, Siegel S, Ansorge RE, Carpenter TA. Preliminary evaluation of a combined microPET-MR system. Technol Cancer Res Treat. 2010;9:53–60.
20. Levin CGG, Deller T, McDaniel D, Peterson W, Maramraju SH. Prototype time-of-flight PET ring integrated with a 3T MRI system for simultaneous whole-body PET/MR imaging. J Nucl Med. 2013;54 Suppl 2:148.
21. Levin CFJ, Deller T, Maramraju SH and Lagaru A. Performance of a high sensitivity time-of-flight PET ring operating simultaneously within a 3T MR system Proceeding of 3rd conferences on PET-MR and SPECT-MR. Kos Island, 19–21 May 2014. 2014.
22. Queiroz MA, Delso G, Wollenweber S, et al. Dose optimization in TOF-PET/MR compared to TOF-PET/CT. PLoS One. 2015;10:e0128842.
23. Wagadarikar I, Dolinsky M. Sensitivity improvement of time-of-flight (ToF) PET detector through recovery of compton scattered annihilation photons. IEEE Trans Nucl Sci. 2014;61:121–5.
24. Balyasnikova S, Lofgren J, de Nijs R, et al. PET/MR in oncology: an introduction with focus on MR and future perspectives for hybrid imaging. Am J Nucl Med Mol Imag. 2012;2:458–74.
25. Keereman V, Mollet P, Berker Y, Schulz V, Vandenberghe S. Challenges and current methods for attenuation correction in PET/MR. MAGMA. 2012;26:81–98.
26. Carrio IR, Pablo R, editors. PET/MRI: methodology and clinical applications. Heidelberg: Springer; 2014.
27. Delso G, Ziegler S. PET/MR system design. In: Ignasi C, Pablo R, editors. PET/MRI: methodology and clinical applications. Heidelberg: Springer; 2014. p. 1–19.
28. Wu Y, Catana C, Farrell R, et al. PET performance evaluation of an MR-compatible PET insert. IEEE Trans Nucl Sci. 2009;56:574–80.
29. Shao Y, Cherry SR, Farahani K, et al. Simultaneous PET and MR imaging. Phys Med Biol. 1997;42:1965–70.
30. Shao Y, Cherry SR, Farahani K, Slates R, Silverman RW, Meadors K, Bowery A, Siegel S, Marsden PK, Garlick PB. Development of a PET detector system compatible with MRI/NMR systems. IEEE Trans Nucl Sci. 1997;44:1167–71.
31. Yamamoto S, Imaizumi M, Kanai Y, et al. Design and performance from an integrated PET/MRI system for small animals. Ann Nucl Med. 2010;24:89–98.
32. Pichler BJ, Judenhofer MS, Catana C, et al. Performance test of an LSO-APD detector in a 7-T MRI scanner for simultaneous PET/MRI. J Nucl Med. 2006;47:639–47.
33. Del Guerra A DN, Bisogni MG, Corsi F, Foresta M, et al. Silicon photomultipliers (SiPM) as novel photodetectors for PET. Nucl. Instrum Methods Phys. Res. A. 2011;648:S232–5
34. Roncali E, Cherry S. Application of silicon photomultipliers to positron emission tomography. Ann Biomed Eng. 2011;39:1358–77.
35. Surti S. Update on time-of-flight PET imaging. J Nucl Med. 2014;56:98–105.
36. Yamamoto S, Kuroda K, Senda M. Scintillator selection for MR-compatible gamma detectors. IEEE Trans Nucl Sci. 2003;50:1683–5.
37. Zaidi HE. Molecular imaging of small animals: instrumentation and applications. New York: Springer; 2014.
38. Khalil M. Positron emission tomography (PET): basic principles. In: Khalil M, editor. Basic sciences of nuclear medicine. Berlin/Heidelberg: Springer; 2011. p. 179–209.
39. Pichler B, Lorenz E, Mirzoyan R, et al. Performance test of a LSO-APD PET module in a 9.4 tesla magnet. IEEE Nuclear Science Symposium Conference Record of the IEEE Nuclear Science Symposium and Medical Imaging Conference Piscataway. IEEE; 1998. p. 1237–9.
40. Disselhorst JA, Bezrukov I, Kolb A, Parl C, Pichler BJ. Principles of PET/MR imaging. J Nucl Med. 2014;55:2S–10.
41. Spanoudaki V, Levin C. Photo-detectors for time of flight positron emission tomography (ToF-PET). Sensors (Basel). 2010;10:10484–505.
42. Catana C, Wu Y, Judenhofer MS, et al. Simultaneous acquisition of multislice PET and MR images: initial results with a MR-compatible PET scanner. J Nucl Med. 2006;47:1968–76.
43. Peng BJ, Wu Y, Cherry SR, Walton JH. New shielding configurations for a simultaneous PET/MRI scanner at 7T. J Magn Reson. 2014;239:50–6.
44. Beyer T, Mawlawi O, Harald Q. PET/MR instrumentation. In: Ratib O, Scwaiger M, Beyer T, editors. Atlas of PET/MR imaging in oncology. Berlin/New York: Springer; 2013.
45. España S, Fraile L, Herraiz J, Udías J, Desco M, Vaquero J. Performance evaluation of SiPM photodetectors for PET imaging in the presence of magnetic fields. Nucl Instrum Methods Phys Res A. 2010;613:308–16.
46. Wehner J, Weissler B, Dueppenbecker P, et al. PET/MRI insert using digital SiPMs: investigation of MR-compatibility. Nucl Instrum Methods Phys Res A. 2014;734:116–21.
47. Ay MR, Mehranian A, Abdoli M, Ghafarian P, Zaidi H. Qualitative and quantitative assessment of metal artifacts arising from implantable cardiac pacing devices in oncological PET/CT studies: a phantom study. Mol Imaging Biol. 2011;13: 1077–87.
48. Weissler B, Gebhardt P, Duppenbecker P, et al. A digital preclinical PET/MRI insert and initial results. IEEE Trans Med Imaging. 2015;34:2258–70.
49. http://mri-q.com/gradient-coils.html. Accessed Nov 2015.

50. Shah SN, Huang SS. Hybrid PET/MR imaging: physics and technical considerations. Abdom Imaging. 2015;40:1358–65.
51. Truhn D, Kiessling F, Schulz V. Optimized RF shielding techniques for simultaneous PET/MR. Med Phys. 2011;38:3995–4000.
52. Duppenbecker PM, Wehner J, Renz W, et al. Gradient transparent RF housing for simultaneous PET/MRI using carbon fiber composites. In: Nuclear Science Symposium and Medical Imaging Conference (NSS/MIC). IEEE; 2012. p. 3478–80.
53. Wolf G, Abolmaali N. Preclinical molecular imaging using PET and MRI. Recent Results Cancer Res. 2012;187:257–310.
54. Yang Y, Wu Y, Qi J, et al. A prototype PET scanner with DOI-encoding detectors. J Nucl Med. 2008;49: 1132–40.
55. Poole M, Bowtell R, Green D, et al. Split gradient coils for simultaneous PET-MRI. Magn Reson Med. 2009;62:1106–11.
56. Vandenberghe S, Marsden PK. PET-MRI: a review of challenges and solutions in the development of integrated multimodality imaging. Phys Med Biol. 2015;60:R115–54.
57. Bindseil GA, Gilbert KM, Scholl TJ, Handler WB, Chronik BA. First image from a combined positron emission tomography and field-cycled MRI system. Magn Reson Med. 2011;66:301–5.
58. Lucas AJ, Hawkes RC, Ansorge RE, et al. Development of a combined microPET-MR system. Technol Cancer Res Treat. 2006;5:337–41.
59. Nagy K, Toth M, Major P, et al. Performance evaluation of the small-animal nanoScan PET/MRI system. J Nucl Med. 2013;54:1825–32.
60. Szanda I, Mackewn J, Patay G, et al. National Electrical Manufacturers Association NU-4 performance evaluation of the PET component of the NanoPET/CT preclinical PET/CT scanner. J Nucl Med. 2011;52:1741–7.
61. Marshall HR, Stodilka RZ, Theberge J, et al. A comparison of MR-based attenuation correction in PET versus SPECT. Phys Med Biol. 2011;56: 4613–29.
62. Teuho J, Johansson J, Linden J, et al. Quantitative bias in PET/MR from attenuation correction and reconstruction: a comparison with PET and PET/CT with an anatomical brain phantom and Hoffman brain phantom. In, Nuclear Science Symposium and Medical Imaging Conference (NSS/MIC). IEEE; 2013. p. 1–8.
63. Meikle SR, Bailey DL, Hooper PK, et al. Simultaneous emission and transmission measurements for attenuation correction in whole-body PET. J Nucl Med. 1995;36:1680–8.
64. deKemp RA, Nahmias C. Attenuation correction in PET using single photon transmission measurement. Med Phys. 1994;21:771–8.
65. Kinahan PE, Townsend DW, Beyer T, Sashin D. Attenuation correction for a combined 3D PET/CT scanner. Med Phys. 1998;25:2046–53.
66. Blankcspoor SC HB, Brown JK, Heanue JA, Gould RG, Cann CE, Dae MW. Development of an emission-transmission CT system combining X-ray CT and SPECT. Conference Record of the 1994 IEEE Nuclear Science Symposium and Medical Imaging Conference. 1994. p. 1758–61.
67. Wagenknecht G, Kaiser HJ, Mottaghy FM, Herzog H. MRI for attenuation correction in PET: methods and challenges. MAGMA. 2012;26:99–113.
68. Malone IB, Ansorge RE, Williams GB, et al. Attenuation correction methods suitable for brain imaging with a PET/MRI scanner: a comparison of tissue atlas and template attenuation map approaches. J Nucl Med. 2011;52:1142–9.
69. Ashburner J, Friston KJ. Nonlinear spatial normalization using basis functions. Hum Brain Mapp. 1999;7:254–66.
70. Kops R, Herzog H. Alternative methods for attenuation correction for PET images in MR-PET scanners. Nuclear Science Symposium Conference Record. Vol 6. NSS'07 IEEE;2007. p. 4327–30.
71. Hofmann M, Steinke F, Scheel V, et al. MRI-based attenuation correction for PET/MRI: a novel approach combining pattern recognition and atlas registration. J Nucl Med. 2008;49:1875–83.
72. Hofmann M, Bezrukov I, Mantlik F, et al. MRI-based attenuation correction for whole-body PET/MRI: quantitative evaluation of segmentation- and atlas-based methods. J Nucl Med. 2011;52:1392–9.
73. Schreibmann E, Nye JA, Schuster DM, et al. MR-based attenuation correction for hybrid PET-MR brain imaging systems using deformable image registration. Med Phys. 2010;37:2101–9.
74. Hofmann M, Pichler B, Scholkopf B, Beyer T. Towards quantitative PET/MRI: a review of MR-based attenuation correction techniques. Eur J Nucl Med Mol Imaging. 2009;36 Suppl 1:S93–104.
75. Visvikis DMF, Bert J, Hatt M, Fayad H. PET/MR attenuation correction: where have we come from and where are we going? Eur J Nucl Med Mol Imaging. 2014;41(6):1172–5.
76. Bezrukov I, Schmidt H, Mantlik F, et al. MR-based attenuation correction methods for improved PET quantification in lesions within bone and susceptibility artifact regions. J Nucl Med. 2013;54:1768–74.
77. Burgos N, Cardoso MJ, Modat M, et al. Attenuation correction synthesis for hybrid PET-MR scanners. Med Image Comput Assist Interv. 2014;16:147–54.
78. Burgos N, Cardoso MJ, Thielemans K, et al. Attenuation correction synthesis for hybrid PET-MR scanners: application to brain studies. IEEE Trans Med Imaging. 2014;33:2332–41.
79. Lois C, Bezrukov I, Schmidt H, et al. Effect of MR contrast agents on quantitative accuracy of PET in combined whole-body PET/MR imaging. Eur J Nucl Med Mol Imaging. 2012;39:1756–66.
80. Zaidi H, Montandon ML, Slosman DO. Magnetic resonance imaging-guided attenuation and scatter corrections in three-dimensional brain positron emission tomography. Med Phys. 2003;30:937–48.

81. Schulz V, Torres-Espallardo I, Renisch S, et al. Automatic, three-segment, MR-based attenuation correction for whole-body PET/MR data. Eur J Nucl Med Mol Imaging. 2010;38:138–52.
82. Akbarzadeh A, Ay MR, Ahmadian A, Alam NR, Zaidi H. MRI-guided attenuation correction in whole-body PET/MR: assessment of the effect of bone attenuation. Ann Nucl Med. 2012;27:152–62.
83. Martinez-Moller A, Souvatzoglou M, Delso G, et al. Tissue classification as a potential approach for attenuation correction in whole-body PET/MRI: evaluation with PET/CT data. J Nucl Med. 2009;50: 520–6.
84. Kim JH, Lee JS, Song IC, Lee DS. Comparison of segmentation-based attenuation correction methods for PET/MRI: evaluation of bone and liver standardized uptake value with oncologic PET/CT data. J Nucl Med. 2012;53:1878–82.
85. Steinberg J, Jia G, Sammet S, et al. Three-region MRI-based whole-body attenuation correction for automated PET reconstruction. Nucl Med Biol. 2010;37:227–35.
86. Delso G, Wiesinger F, Sacolick LI, et al. Clinical evaluation of zero-echo-time MR imaging for the segmentation of the skull. J Nucl Med. 2015;56:417–22.
87. Catana C, van der Kouwe A, Benner T, et al. Toward implementing an MRI-based PET attenuation-correction method for neurologic studies on the MR-PET brain prototype. J Nucl Med. 2010;51: 1431–8.
88. Bezrukov I, Mantlik F, Schmidt H, Scholkopf B, Pichler BJ. MR-Based PET attenuation correction for PET/MR imaging. Semin Nucl Med. 2013;43:45–59.
89. Gibiino F, Sacolick L, Menini A, Landini L, Wiesinger F. Free-breathing, zero-TE MR lung imaging. MAGMA. 2014;28:207–15.
90. Roy S, Wang WT, Carass A, et al. PET attenuation correction using synthetic CT from ultrashort echo-time MR imaging. J Nucl Med. 2014;55:2071–7.
91. Keereman V, Fierens Y, Broux T, et al. MRI-based attenuation correction for PET/MRI using ultrashort echo time sequences. J Nucl Med. 2010;51:812–8.
92. Berker Y, Franke J, Salomon A, et al. MRI-based attenuation correction for hybrid PET/MRI systems: a 4-class tissue segmentation technique using a combined ultrashort-echo-time/Dixon MRI sequence. J Nucl Med. 2012;53:796–804.
93. Aasheim LB, Karlberg A, Goa PE, et al. PET/MR brain imaging: evaluation of clinical UTE-based attenuation correction. Eur J Nucl Med Mol Imaging. 2015;42:1439–46.
94. Rezaei A, Defrise M, Bal G, et al. Simultaneous reconstruction of activity and attenuation in time-of-flight PET. IEEE Trans Med Imaging. 2012;31:2224–33.
95. Conti M. Focus on time-of-flight PET: the benefits of improved time resolution. Eur J Nucl Med Mol Imaging. 2011;38:1147–57.
96. Torigian DA, Zaidi H, Kwee TC, et al. PET/MR imaging: technical aspects and potential clinical applications. Radiology. 2013;267:26–44.
97. Bashir U, Mallia A, Stirling J, et al. PET/MRI in oncological imaging: state of the art. Diagnostics (Basel). 2015;5(3):333–57.
98. von Schulthess GK, Veit-Haibach P. Workflow considerations in PET/MR imaging. J Nucl Med. 2014; 55:19S–24.
99. Drzezga A, Souvatzoglou M, Eiber M, et al. First clinical experience with integrated whole-body PET/MR: comparison to PET/CT in patients with oncologic diagnoses. J Nucl Med. 2014;53:845–55.
100. Schramm G, Langner J, Hofheinz F, et al. Quantitative accuracy of attenuation correction in the Philips Ingenuity TF whole-body PET/MR system: a direct comparison with transmission-based attenuation correction. MAGMA. 2013;26: 115–26.
101. Izquierdo-Garcia D, Sawiak SJ, Knesaurek K, et al. Comparison of MR-based attenuation correction and CT-based attenuation correction of whole-body PET/MR imaging. Eur J Nucl Med Mol Imaging. 2014;41:1574–84.
102. Nehmeh SA, Erdi YE. Respiratory motion in positron emission tomography/computed tomography: a review. Semin Nucl Med. 2008;38:167–76.
103. Ai H, Pan T. Feasibility of using respiration-averaged MR images for attenuation correction of cardiac PET/MR imaging. J Appl Clin Med Phys. 2015; 16(4):5194.
104. Petibon Y, Huang C, Ouyang J, et al. Relative role of motion and PSF compensation in whole-body oncologic PET-MR imaging. Med Phys. 2014;41:042503.
105. Guerin B, Cho S, Chun SY, et al. Nonrigid PET motion compensation in the lower abdomen using simultaneous tagged-MRI and PET imaging. Med Phys. 2011;38:3025–38.
106. Lamare F, Ledesma Carbayo MJ, Cresson T, et al. List-mode-based reconstruction for respiratory motion correction in PET using non-rigid body transformations. Phys Med Biol. 2007;52:5187–204.
107. Rahmim ABP, Houle S, Lenox M, Michel C, Buckley KR, Ruth TJ, Sossi V. Motion compensation in histogram-mode and list-mode EM reconstructions: beyond the event-driven approach. IEEE Trans Nucl Sci. 2004;51(5):2588–96.
108. Reyes M, Malandain G, Koulibaly PM, Gonzalez-Ballester MA, Darcourt J. Model-based respiratory motion compensation for emission tomography image reconstruction. Phys Med Biol. 2007;52:3579–600.
109. Attenberger U, Catana C, Chandarana H, et al. Whole-body FDG PET-MR oncologic imaging: pitfalls in clinical interpretation related to inaccurate MR-based attenuation correction. Abdom Imaging. 2015;40:1374–86.
110. Bryant D, Payne J, Firmin D, Longmore D. Measurement of flow with NMR imaging using a gradient pulse and phase difference technique. J Comput Assist Tomogr. 1984;8:588–93.
111. Würslin CSH, Martirosian P, Brendle C, Boss A, Schwenzer NF, Stegger L. Respiratory motion correction in oncologic PET using T1-weighted MR

imaging on a simultaneous whole-body PET/MR system. J Nucl Med. 2013;54(3):464–71.
112. Manber R, Thielemans K, Hutton BF, et al. Practical PET respiratory motion correction in clinical PET/MR. J Nucl Med. 2015;56:890–6.
113. Grimm R, Furst S, Souvatzoglou M, et al. Self-gated MRI motion modeling for respiratory motion compensation in integrated PET/MRI. Med Image Anal. 2014;19:110–20.
114. Ouyang J, Petibon Y, Huang C, et al. Quantitative simultaneous positron emission tomography and magnetic resonance imaging. J Med Imaging (Bellingham). 2014;1:033502.
115. Bagade S, Fowler KJ, Schwarz JK, Grigsby PW, Dehdashti F. PET/MRI evaluation of gynecologic malignancies and prostate cancer. Semin Nucl Med. 2015;45:293–303.
116. Pearce MS, Salotti JA, Little MP, et al. Radiation exposure from CT scans in childhood and subsequent risk of leukaemia and brain tumours: a retrospective cohort study. Lancet. 2012;380:499–505.
117. Bai B, Li Q, Leahy RM. Magnetic resonance-guided positron emission tomography image reconstruction. Semin Nucl Med. 2012;43:30–44.
118. Mehranian A, Zaidi H. Emission-based estimation of lung attenuation coefficients for attenuation correction in time-of-flight PET/MR. Phys Med Biol. 2015;60:4813–33.
119. Mehranian A, Zaidi H. Clinical assessment of emission- and segmentation-based MR-guided attenuation correction in whole-body time-of-flight PET/MR imaging. J Nucl Med. 2015;56:877–83.
120. Fei B, Yang X, Nye JA, et al. MRPET quantification tools: registration, segmentation, classification, and MR-based attenuation correction. Med Phys. 2012;39:6443–54.
121. Fluckiger J, Li X, Whisenant J, et al. Using dynamic contrast-enhanced magnetic resonance imaging data to constrain a positron emission tomography kinetic model: theory and simulations. Int J Biomed Imaging. 2013;2013:576470.
122. Su Y, Blazey T, Snyder A, et al. Quantitative amyloid imaging using image-derived arterial input function. PLoS One. 2015;10:e0122920.
123. Wehrl HF, Hossain M, Lankes K, et al. Simultaneous PET-MRI reveals brain function in activated and resting state on metabolic, hemodynamic and multiple temporal scales. Nat Med. 2013;19:1184–9.
124. Sander CY, Hooker JM, Catana C, et al. Neurovascular coupling to D2/D3 dopamine receptor occupancy using simultaneous PET/functional MRI. Proc Natl Acad Sci U S A. 2013;110:11169–74.
125. Bruehlmeier M, Roelcke U, Schubiger PA, Ametamey SM. Assessment of hypoxia and perfusion in human brain tumors using PET with 18F-fluoromisonidazole and 15O-H2O. J Nucl Med. 2004;45:1851–9.
126. Rauscher I, Eiber M, Souvatzoglou M, Schwaiger M, Beer AJ. PET/MR in oncology: non-18F-FDG tracers for routine applications. J Nucl Med. 2014;55:25S–31.
127. Yang X, Hong H, Grailer JJ, et al. cRGD-functionalized, DOX-conjugated, and (6)(4) Cu-labeled superparamagnetic iron oxide nanoparticles for targeted anticancer drug delivery and PET/MR imaging. Biomaterials. 2011;32:4151–60.
128. Covello M, Cavaliere C, Aiello M, et al. Simultaneous PET/MR head-neck cancer imaging: preliminary clinical experience and multiparametric evaluation. Eur J Radiol. 2015;84:1269–76.
129. Catana C, Guimaraes AR, Rosen BR. PET and MR imaging: the odd couple or a match made in heaven? J Nucl Med. 2013;54:815–24.
130. Lee SI, Catalano OA, Dehdashti F. Evaluation of gynecologic cancer with MR imaging, 18F-FDG PET/CT, and PET/MR imaging. J Nucl Med. 2015;56:436–43.
131. Catalano OA, Nicolai E, Rosen BR, et al. Comparison of CE-FDG-PET/CT with CE-FDG-PET/MR in the evaluation of osseous metastases in breast cancer patients. Br J Cancer. 2015;112:1452–60.
132. Gaeta CM, Vercher-Conejero JL, Sher AC, et al. Recurrent and metastatic breast cancer PET, PET/CT, PET/MRI: FDG and new biomarkers. Q J Nucl Med Mol Imaging. 2013;57:352–66.
133. Floriani I, Torri V, Rulli E, et al. Performance of imaging modalities in diagnosis of liver metastases from colorectal cancer: a systematic review and meta-analysis. J Magn Reson Imaging. 2009;31:19–31.
134. Niekel MC, Bipat S, Stoker J. Diagnostic imaging of colorectal liver metastases with CT, MR imaging, FDG PET, and/or FDG PET/CT: a meta-analysis of prospective studies including patients who have not previously undergone treatment. Radiology. 2010;257:674–84.
135. Barthel H, Schroeter ML, Hoffmann KT, Sabri O. PET/MR in dementia and other neurodegenerative diseases. Semin Nucl Med. 2015;45:224–33.
136. Drzezga A, Barthel H, Minoshima S, Sabri O. Potential clinical applications of PET/MR imaging in neurodegenerative diseases. J Nucl Med. 2014;55:47S–55.
137. Fink J, Muzi M, Peck M, Krohn KA. Multi-modality brain tumor imaging – MRI, PET, and PET/MRI. J Nucl Med. 2015;56:1554–61.
138. Ratib O, Nkoulou R. Potential applications of PET/MR imaging in cardiology. J Nucl Med. 2014;55:40S–6.
139. Nappi C, El Fakhri G. State of the art in cardiac hybrid technology: PET/MR. Curr Cardiovasc Imaging Rep. 2013;6:338–45.